PAPER

Check for updates

Investigation of slow magnetic relaxation in a series of 1D polymeric cyclobutane-1,1-dicarboxylates based on Ln^III V_2^IV units (Ln^III = Tb, Dy, Ho, Er, Tm, Yb): rare examples of V^IV-4f single-molecule magnets†

Evgeniya S. Bazhina, [ID] *[a] Maxim A. Shmelev, [ID] [a] Natalia V. Gogoleva, [ID] [a] Konstantin A. Babeshkin, [ID] [a] Ivan V. Kurganskii, [ID] [b] Nikolay N. Efimov, [ID] [a] Matvey V. Fedin, [ID] [b] Mikhail A. Kiskin [ID] [a] and Igor L. Eremenko [ID] [a]

The reactions of $VOSO_4 \cdot 3H_2O$ with $Na_2(cbdc)$ ($cbdc^{2-}$ – dianion of cyclobutane-1,1-dicarboxylic acid) and lanthanide(III) nitrates taken in a molar ratio of 1 : 2 : 1 were found to yield a series of isostructural heterometallic compounds $[NaLn(VO)_2(cbdc)_4(H_2O)_{10}]_n$ (**1_Ln**, Ln = Tb, Dy, Ho, Er, Tm, Yb). These compounds are constructed from trinuclear anionic units $[Ln(VO)_2(cbdc)_4(H_2O)_8]^-$ ({LnV_2}^-) linked by Na^+ ions into 1D polymeric chains. The crystal structures of **1_Dy** and **1_Er** were determined by single-crystal X-ray diffraction (XRD), and their isostructurality with **1_Tb**, **1_Ho**, **1_Tm**, and **1_Yb** was proved by powder X-ray diffraction (PXRD). According to alternating current (ac) magnetic susceptibility measurements, **1_Dy**, **1_Er**, and **1_Yb** exhibited field-induced slow relaxation of magnetization. Compound **1_Er** is the first representative of Er^III–V^IV single-molecule magnets. Measuring the temperature dependences of the phase memory time (T_m) for **1_Dy** and **1_Yb** using pulsed EPR spectroscopy allowed us to observe the phenomenon of phase relaxation enhancement (PRE) at temperatures below 30 K. In future, this phenomenon may contribute to the evaluation of relaxation times of the lanthanide ions.

[a]*N.S. Kurnakov Institute of General and Inorganic Chemistry, Russian Academy of Sciences, Leninsky prosp. 31, Moscow 119991, Russian Federation. E-mail: bazhina@igic.ras.ru*

[b]*International Tomography Center, Siberian Branch of Russian Academy of Sciences, Institutskaya St. 3a, Novosibirsk 630090, Russian Federation*

†Electronic supplementary information (ESI) available: Orbital diagrams for Cu^II and V^IV ions; PXRD patterns for **1_Ln** series; continuous shape measures (CShM) for LnO_8 coordination polyhedra in **1_Dy**, **1_Er**; tables of selected bond angles in structures **1_Dy**, **1_Er**; tables of hydrogen bond parameters in **1_Dy**, **1_Er**; the magnetization $M(T)$ and $M(H/T)$ dependences for **1_Ln**, frequency dependences of the in-phase and out-of-phase parts of dynamic magnetic susceptibility for **1_Ln** at $T = 2$ K under various dc-magnetic fields; frequency dependences of the in-phase and out-of-phase parts of dynamic magnetic susceptibility for **1_Dy**, **1_Er**, **1_Tm** (under 1000 Oe dc-field), and **1_Yb** (under 2500 Oe dc-field) at different temperatures; Cole–Cole plots for **1_Dy** measured at 2–7.5 K; the τ *vs. H* plots for **1_Dy**, **1_Er**, **1_Yb** at 2 K; the τ *vs.* $1/T$ plots and the best-fit parameters of magnetization relaxation for **1_Tm**; the τ *vs.* $1/T$ plots for **1_Dy**, **1_Er**, **1_Yb** processed using the MagSuite v.3.2 software and the best-fit parameters of magnetization relaxation calculated for **1_Dy**, **1_Er**, **1_Yb**; CW EPR spectra of M_Y and 1_Y at 293 K and 10 K; IR spectra for **1_Dy** in aqueous solution and crystalline state. CCDC 2266768 and 2266772. For ESI and crystallographic data in CIF or other electronic format see DOI: https://doi.org/10.1039/d4dt01779j

Introduction

Effective ways for the synthesis of heterometallic 3d–4f coordination compounds exhibiting properties of a bulk magnet at the molecular level are currently being developed.[1] While constructing such complex molecules, paramagnetic 3d-metal ions are used, which are often involved in spin–spin exchange interactions *via* a super-exchange mechanism through a diamagnetic bridging ligand.[2] Thus, the value of the exchange parameter affects the relaxation characteristics of a single-molecule magnet (SMM): strong exchange interactions enable reduction of the contribution of quantum tunneling of magnetization (QTM) to the relaxation of magnetization, increasing the value of the energy barrier for magnetization reversal, while the presence of weak and dipole–dipole interactions in the compound reduces the value of this parameter.[3]

Among all known SMMs based on heterometallic 3d–4f systems, the magnetic properties of Cu^II–Ln^III complexes are the most well-studied; the influence of the geometric characteristics of the molecule on the parameter of exchange interactions was shown for these compounds.[4] Similar to Cu^II, the V^IV ion also has $S = 1/2$, however, the electronic structure of

these ions is different: a single unpaired electron of V^{IV} is located on the d_{xy} orbital, but not on the $d_{x^2-y^2}$ orbital, as in the case of Cu^{II} (Fig. S1†).[5] In this regard, Cu^{II}–Ln^{III} and V^{IV}–Ln^{III} compounds cannot be expected to exhibit identical magnetic properties. In addition, the geometric features of the $V^{IV}O^{2+}$ ion, *i.e.* the presence of an oxo group, exclude the formation of V^{IV}–Ln^{III} compounds similar in structure to their analogues containing the ions of Cu^{II} and other divalent 3d-metals. Despite ongoing studies of V^{IV}–Ln^{III} complexes, very few such compounds exhibiting SMM properties have been obtained so far.[6] Therefore, the synthesis and detailed study of the magnetic properties of V^{IV}–Ln^{III} systems is an urgent task of modern coordination chemistry. The presence of a single unpaired d-electron also gives rise to the interest in V^{IV} compounds as potential candidates for molecular-based spin qubits[7] and makes them convenient objects for the study by EPR spectroscopy.

On the other hand, it is of interest to study 3d–4f SMMs containing lanthanide ions rarely used for these purposes, for example, Er^{III} and Yb^{III} (see ref. 8) or non-Kramers lanthanide ions, Ho^{III} and Tm^{III} (see ref. 9 and 10), for which the coordination environment is of great importance to control the magnetic anisotropy. To date, 3d–4f SMMs with Ho^{III}, Er^{III}, Tm^{III}, and Yb^{III} ions still remain much less studied than their Tb^{III} and Dy^{III}-containing counterparts.

Polydentate ligands that combine chelation with a variety of bridging coordination modes enable the constructing stable anionic blocks with atoms of 3d-elements and binding them with 4f-metal ions in a polynuclear molecule or coordination polymer without the use of additional ligands. An additional factor in the design of 3d–4f compounds can be the alkali metal ions introduced at the synthesis stage, which are diamagnetic, but often play a structure-directing role in the formation of the structure in the crystal, and therefore can influence the molecular geometry of the complex and, in particular, the coordination environment of paramagnetic metal centers. The structure-directing role of alkali metal ions has been studied for coordination polymers of s-elements,[11] heteronuclear compounds of s-3d (see ref. 12) and s-4f metals.[13] Very few such studies are known for heterometallic 3d–4f systems.[14]

In our previous studies, we investigated the influence of the ionic radii of M^I (M = Na, K, Rb, Cs) and Ln^{III} on the composition, structure, and magnetic properties of heterometallic compounds formed in the M^I–Ln^{III}–V^{IV} systems with anions of cyclobutane-1,1-dicarboxylic acid (H_2cbdc).[6a,c,15] According to X-ray diffraction studies, alkali metal ions in this series of compounds affect not only the crystal packing of the compound, but also the geometric characteristics of the Ln^{III}–V^{IV} molecular fragments that form it, and, as a consequence, the exhibited magnetic properties. For Na^I, the formation of 1D polymeric structures $[NaLn(VO)_2(cbdc)_4(H_2O)_{10}]_n$ was found in the systems with diamagnetic rare-earth metal ions Y^{III} and Lu^{III} (see ref. 16), as well as with Gd^{III} (see ref. 15).

The present work is the logical continuation of our previous research, so it sets out to synthesize heterometallic Na^I–Ln^{III}–V^{IV} compounds with paramagnetic lanthanide ions from Tb^{III}

to Yb^{III} having high magnetic anisotropy and to study the slow magnetic relaxation phenomenon in the resulting complexes.

Results and discussion

Synthesis

The reactions of aqueous oxovanadium(IV) nitrate (prepared *via* metathesis between $VOSO_4·3H_2O$ and $Ba(NO_3)_2$ in water), $Na_2(cbdc)$ and lanthanide(III) nitrates (Tb^{III}, Dy^{III}, Ho^{III}, Er^{III}, Tm^{III}, Yb^{III}) in a molar ratio of 1 : 2 : 1 yielded blue crystals of a series of heterometallic compounds $[NaLn(VO)_2(cbdc)_4(H_2O)_{10}]_n$ ($\mathbf{1_{Ln}}$). Barium nitrate was added to the reaction mixture to remove sulfate anions from the solution, because the presence of these anions causes the crystallization of Ln^{III} sulfates.

The description of crystal structures

According to PXRD data, all $\mathbf{1_{Ln}}$ compounds are isostructural (Fig. S2 in ESI†). The crystal structures of $\mathbf{1_{Dy}}$ and $\mathbf{1_{Er}}$ were determined by single-crystal XRD. Compounds $\mathbf{1_{Dy}}$ and $\mathbf{1_{Er}}$ crystallize in monoclinic space group $C2/c$. The asymmetric units of $\mathbf{1_{Dy}}$ and $\mathbf{1_{Er}}$ contain one vanadium atom (V1), one lanthanide atom (Dy1 or Er1), and one sodium atom (Na1). In addition to the vanadyl oxo group, V1 atom coordinates two chelating $cbdc^{2-}$ anions and one water molecule, thus forming mononuclear bis-chelate $\{VO(cbdc)_2(H_2O)\}^{2-}$ moiety.

The geometry of vanadium coordination polyhedron is a distorted octahedron (VO_6) whose equatorial plane is formed by four carboxylate O atoms. The O atoms of the oxo group and water molecule occupy the axial positions and form the shortened (~1.60 Å) and the elongated (~2.30 Å) bonds with a metal center, respectively (Fig. 1 and Table 1). The V1 atom deviates from the equatorial plane by 0.371 Å (in $\mathbf{1_{Dy}}$) and 0.374 Å (in $\mathbf{1_{Er}}$) towards oxo group, giving rise to the increase of V=O/V–O(cbdc) bond angles and the decrease of V–O(cbdc)/V–O(H_2O) ones (Table 2).

Each lanthanide atom binds to the two $\{VO(cbdc)_2(H_2O)\}^{2-}$ moieties *via* the coordination of two unchelated carboxylate O atoms. In the resulting $\{LnV_2\}^-$ trinuclear unit, the central lanthanide atom additionally coordinates six water molecules completing its polyhedron having the geometry of a triangular dodecahedron (TDD-8, the deviations from the ideal figure, CShM values are 0.630 and 0.640 for $\mathbf{1_{Dy}}$ and $\mathbf{1_{Er}}$ respectively) (see Table S1 in the ESI†).[17] Selected bond angles in the coordination polyhedra of lanthanides in structures $\mathbf{1_{Dy}}$ and $\mathbf{1_{Er}}$ are given in Tables S2 and S3 in the ESI†.

The neighboring $[Ln(VO)_2(cbdc)_4(H_2O)_8]^-$ units are linked into a 1D polymeric structure due to the coordination of Na atoms to the carboxylate O atoms involved in the chelation of vanadium (Fig. 1 and Table 1). Each Na atom coordinates two monodentate water molecules. The crystal structures of $\mathbf{1_{Dy}}$ and $\mathbf{1_{Er}}$ are additionally stabilized by the network of hydrogen bonds, whose formation involves all the coordinated water molecules, the carboxylate O atoms, and vanadyl oxo group (Tables S4 and S5 in the ESI†).
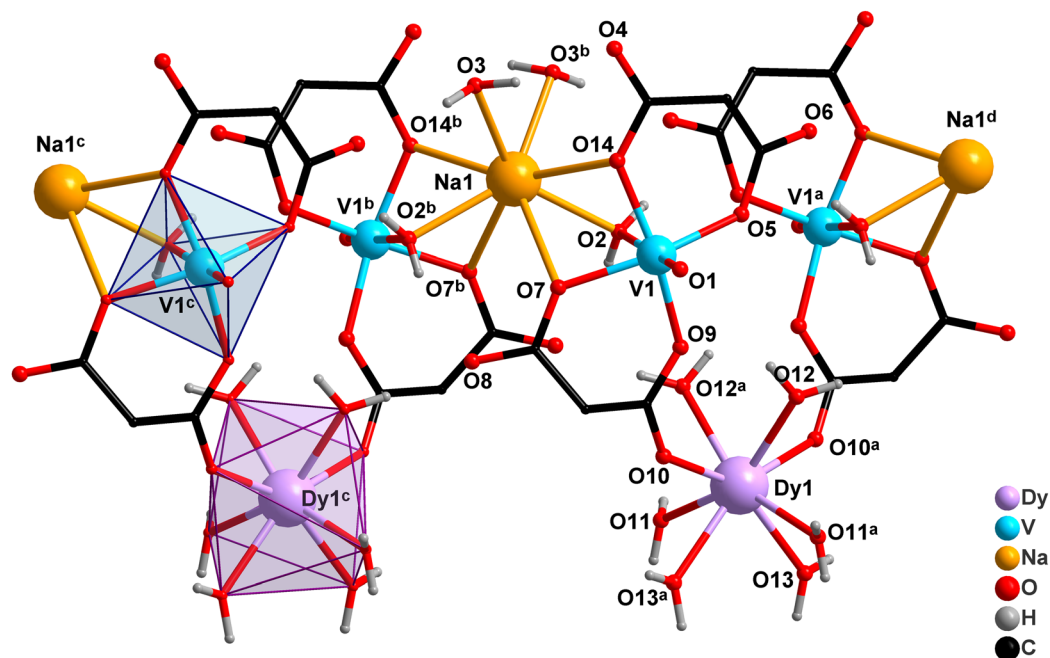
Fig. 1 The fragment of the 1D polymeric chain of 1_{Dy} (cyclobutane moieties are omitted for clarity) [symmetry codes: (a) $1 - x$, y, $0.5 - z$; (b) $-x$, y, $0.5 - z$; (c) $-1 + x$, y, z; (d) $1 + x$, y, z].

Table 1 Selected bond lengths and the shortest interatomic distances (d, Å) in structures 1_{Dy} and 1_{Er}

Compound Bond/distance	1_{Dy} (Ln = Dy)	d	1_{Er} (Ln = Er)
V═O	1.600(2)		1.602(4)
V–O(cbdc)	1.965(2)–2.024(2)		1.965(4)–2.024(4)
V–O(H₂O)	2.299(2)		2.310(4)
Ln–O(cbdc)	2.361(2)		2.335(3)
Ln–O(H₂O)	2.349(2)–2.384(2)		2.317(4)–2.372(4)
Na–O(cbdc)	2.536(2), 2.637(2)		2.530(4), 2.638(4)
Na–O(H₂O)	2.411(2), 2.447(2)		2.413(4), 2.449(4)
Ln⋯V	5.719(1)		5.699(2)
V⋯V	6.245(1)		6.249(3)

Table 2 Selected bond angles (ω, °) characterizing the coordination polyhedra of vanadium in complexes 1_{Dy} and 1_{Er}

Compound Angle	1_{Dy}	ω	1_{Er}
V═O/V–O(cbdc)	100.00(10)–101.90(11)		99.98(18)–102.08(18)
V═O/V–O(H₂O)	177.65(10)		177.91(18)
V–O(cbdc)/ V–O(cbdc) (acute)	85.62(9)–90.12(8)		85.39(15)–90.24(15)
V–O(cbdc)/ V–O(H₂O) (acute)	76.84(8)–81.88(8)		76.76(14)–81.73(14)

Magnetic properties

The magnetic properties of the series of isostructural compounds 1_{Ln} (Ln = Tb, Dy, Ho, Er, Tm, Yb) were studied by measuring the temperature dependences of molar magnetic susceptibility (χ) in the 2–300 K temperature range under 5000 Oe dc-magnetic field. For all compounds, the experimental χT values at 300 K are in satisfactory agreement with theoretical

ones for two magnetically isolated V^{IV} ions and one Ln^{III} ion (Table 3). For Tb^{III}, Dy^{III}, Ho^{III}, Er^{III}, and Tm^{III}-containing compounds, the χT values at 300 K slightly exceed the theoretical ones, but generally fit into the range of acceptable deviations (about 10% from the corresponding theoretical χT value).

For 1_{Dy}, 1_{Ho}, 1_{Er} (Fig. 2), the χT values monotonously decrease in the range from 300 to 100 K and then gradually decrease with decreasing temperature. On cooling below 10 K, the χT values sharply drop and reach a minimum at 2 K.

For 1_{Tb}, a monotonous increase in the χT is observed in the range from 300 to 30 K, probably indicating the presence of weak ferromagnetic interactions. It should be noted that the field-induced orientation of polycrystals was excluded by using the mineral oil during the sample preparation (see Experimental part). With a further decrease in temperature, a sharp decrease in the χT value occurs, reaching a minimum at 2 K. For 1_{Tm}, the χT value remains virtually constant up to 16 K and then sharply decrease with a further decrease in temperature down to 2 K.

Table 3 The χT values for 1_{Ln} under 5000 Oe field

Compound	χT (theor.), cm³ K mol⁻¹	χT (300 K), cm³ K mol⁻¹	χT (2 K), cm³ K mol⁻¹
1_{Tb} ($Tb^{III}V_2^{IV}$)	12.58	13.74	6.76
1_{Dy} ($Dy^{III}V_2^{IV}$)	14.93	15.06	8.49
1_{Ho} ($Ho^{III}V_2^{IV}$)	14.83	15.15	4.68
1_{Er} ($Er^{III}V_2^{IV}$)	12.24	12.53	6.58
1_{Tm} ($Tm^{III}V_2^{IV}$)	7.91	8.60	6.69
1_{Yb} ($Yb^{III}V_2^{IV}$)	3.33	3.37	2.24
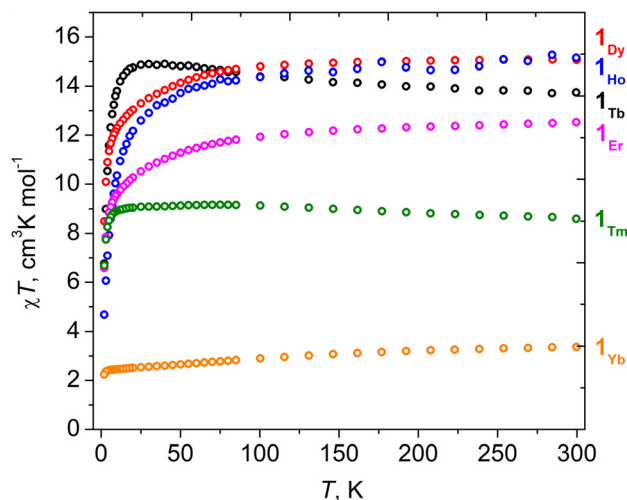
Fig. 2 The experimental χT vs. T plots for compounds $\mathbf{1_{Ln}}$ in the range of 2–300 K under 5000 Oe field.
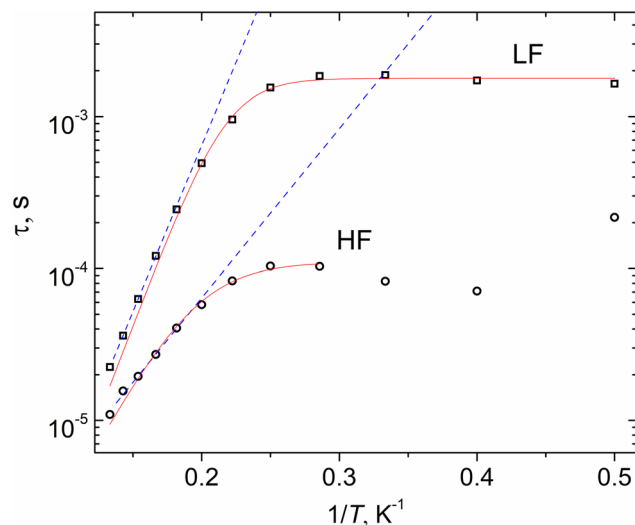

Fig. 3 The τ vs. $1/T$ plots for $\mathbf{1_{Dy}}$ under 1000 Oe field. Blue dashed lines represent the fittings of high-temperature ranges by the Orbach mechanism. Red solid lines represent the fittings in the whole temperature range by the sum of the Orbach and QTM relaxation mechanisms.
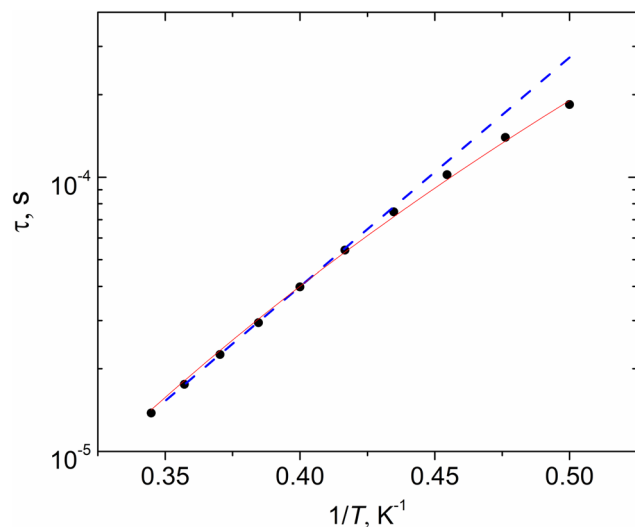

Fig. 4 The τ vs. $1/T$ plots for $\mathbf{1_{Er}}$ under 1000 Oe field. Blue dotted line represents the fitting of a high-temperature range by the Orbach mechanism. Red solid line represents the fitting by the Raman relaxation mechanism.

For $\mathbf{1_{Yb}}$, a monotonous decrease in the χT value is observed in the range from 300 to 2 K. Such a behavior of the compounds under study can be due to the possible presence of spin–spin antiferromagnetic interactions and/or the depopulation of the excited Stark sublevels.[18] The $M(H)$ and $M(H/T)$ dependences for all obtained complexes were also measured at 2, 4, and 6 K (Fig. S3–S6 in the ESI†).

In order to study magnetization relaxation of the compounds, ac-magnetic susceptibility measurements were carried out. In the absence of a dc-magnetic field, the values of the out-of-phase component of dynamic magnetic susceptibility (χ'') were close to zero for all the compounds, which may be due to a strong contribution from quantum tunneling to the relaxation of magnetization. Application of an external dc-field enabled to significantly reduce this effect and observe the χ'' non-zero values for $\mathbf{1_{Dy}}$, $\mathbf{1_{Er}}$, $\mathbf{1_{Tm}}$, and $\mathbf{1_{Yb}}$ (Fig. S7–S12 in the ESI†).

The highest relaxation times were achieved on applying the optimal fields of 1000 Oe for $\mathbf{1_{Dy}}$, $\mathbf{1_{Er}}$, $\mathbf{1_{Tm}}$, and 2500 Oe for $\mathbf{1_{Yb}}$ (Fig. S13–S15†). To produce the τ vs. $1/T$ plots, the $\chi''(\nu)$ isotherms were approximated by the generalized Debye model (Fig. S16–S19 in the ESI†). The plots of τ vs. $1/T$ thus obtained were approximated by the equations corresponding to different relaxation mechanisms and their combinations. In the high-temperature range, all the τ vs. $1/T$ dependences were approximated using only the Orbach relaxation mechanism ($\tau^{-1} = \tau_0^{-1}\cdot\exp\{-\Delta_{\text{eff}}/k_{\text{B}}T\}$) to estimate the value of the effective energy barrier (Fig. 3, 4 and 5).

According to the approximation of χ'' vs. ν dependencies by the generalized Debye model (Fig. S16†), there are at least two or even more relaxation processes for complex $\mathbf{1_{Dy}}$ also confirmed by Cole–Cole plots (Fig. S20 in the ESI†). This may be due to the independent relaxation of Dy$^{\text{III}}$ and V$^{\text{IV}}$ ions[19] and/ or possible disorder of water molecules coordinated to Dy$^{\text{III}}$ (see ref. 14c and 20). Unfortunately, we failed to obtain iso-

structural analogue of complex $\mathbf{1_{Dy}}$ with diamagnetic d-metal ions (Zn$^{\text{II}}$, Cd$^{\text{II}}$), so it was impossible to evaluate the contribution of Dy$^{\text{III}}$ ions to the magnetic relaxation dynamics of complex $\mathbf{1_{Dy}}$. Previously, the magnetic properties of isostructural complexes [NaLn(VO)$_2$(cbdc)$_4$(H$_2$O)$_{10}$]$_n$ with diamagnetic rare-earth ions (Ln = Y$^{\text{III}}$, Lu$^{\text{III}}$) were studied.[16] In both complexes, the presence of field-induced slow relaxation of magnetization was shown by ac-susceptibility measurements. This suggests the contribution of V$^{\text{IV}}$ ions to the magnetic relaxation dynamics in the case of complex $\mathbf{1_{Dy}}$. Therefore, τ vs. $1/T$
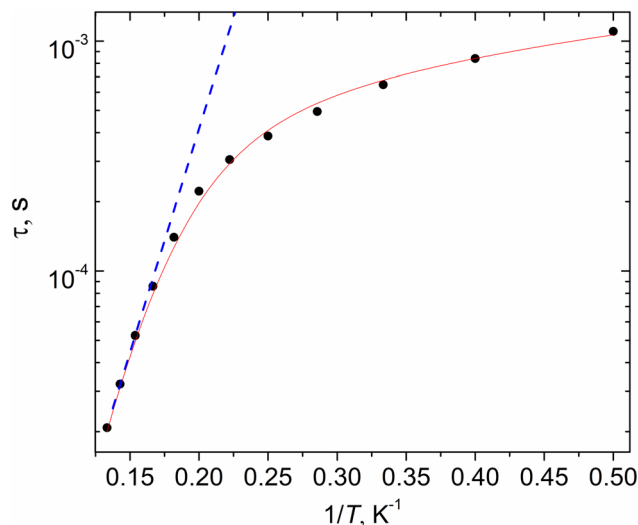
Fig. 5 The τ vs. $1/T$ plots for $1_{\mathbf{Yb}}$ under 2500 Oe field. Blue dotted line represents the fitting of a high-temperature range by the Orbach mechanism. Red solid line represents the fitting by the sum of the Raman and direct relaxation mechanisms.

plots for $1_{\mathbf{Dy}}$ were built using both low-frequency (LF) and high-frequency (HF) maxima of χ'' vs. ν dependencies (Fig. 3). The good agreement between the experimental τ vs. $1/T$ plots and approximation equation can be achieved using parameters for the sum of the Orbach and QTM relaxation mechanisms ($\tau^{-1} = \tau_0^{-1} \cdot \exp\{-\Delta_{\mathrm{eff}}/k_B T\} + B$) both for LF and HF (Table 4).

For $1_{\mathbf{Yb}}$, the best-fit of the experimental τ vs. $1/T$ dependence in the whole temperature range was achieved by the sum of the Raman and direct relaxation mechanisms according to the equation $\tau^{-1} = C_{\mathrm{Raman}}T^{n\_\mathrm{Raman}} + A_{\mathrm{direct}}TH^4$ (Fig. 5). For $1_{\mathbf{Er}}$, the corresponding fit was achieved with the use of only the Raman relaxation mechanism ($\tau^{-1} = C_{\mathrm{Raman}}T^{n\_\mathrm{Raman}}$) (Fig. 4).

For $1_{\mathbf{Tm}}$, the χ'' values are less than the χ' ones by more than 10 times (but χ'/χ'' ratio is close to 10), thus the presence of slow relaxation of magnetization is questionable in this case. All obtained magnetic relaxation data for $1_{\mathbf{Tm}}$ is presented in the ESI (Fig. S21 and Table S6†).

The best-fit parameters for the approximations of τ vs. $1/T$ plots obtained for $1_{\mathbf{Er}}$ and $1_{\mathbf{Yb}}$ are given in Table 5.

It is worth pointing out that for $1_{\mathbf{Er}}$, the value of $n_{\mathrm{Raman}} = 7$ is lower than the expected value for the Kramers systems ($n = 9$), indicating the presence of a Raman process through spin-phonon relaxation.[21]

In addition, for all compounds, the calculations of alternative magnetic relaxation parameters were performed using MagSuite v.3.2 software.[22] The results obtained are presented in Fig. S22–S24 and Tables S7–S9.†

The first V^{IV}–Dy^{III} SMM was described by K. Kotrle et al. (see ref. 6b), but the authors failed to determine possible relaxation mechanisms and estimate the effective energy barrier for this compound. The literature review showed that the value of $\Delta_{\mathrm{eff}}/k_B$ calculated for $1_{\mathbf{Dy}}$ is higher than those for the most known 3d-Dy^{III} SMMs with paramagnetic 3d-metal ions and a similar triangular dodecahedral DyO_8 coordination environment (Table 6).

Considering the previously obtained magnetic data for potassium-containing analogues of $1_{\mathbf{Dy}}$ and $1_{\mathbf{Yb}}$ (see ref. 6a), it can be concluded that in V^{IV}–Ln^{III} systems with cbdc^{2-}, the substitution of potassium by sodium ions giving rise to a significant change in the crystal structure and coordination environment of the lanthanide ion has a positive influence on their SMM behavior. For $1_{\mathbf{Dy}}$, the appearance of slow magnetic relaxation is observed compared to K^I–V^{IV}–Dy^{III} compound. One of the possible explanations for such differences in the magnetic behavior of two Dy-containing compounds may be the difference in Dy^{III} coordination polyhedra, which is a biaugmented trigonal prism (C_{2v} symmetry) in K^I–Dy^{III}–V^{IV} and a triangular dodecahedron (D_{2d} symmetry) in $1_{\mathbf{Dy}}$. Another factor influencing SMM behavior is supposed to be the longer $Dy\cdots V$ distances in $1_{\mathbf{Dy}}$ (5.719 Å) compared to K^I–V^{IV}–Dy^{III} (4.627 Å), that allow weakening of dipole–dipole interactions between Dy^{III} and V^{IV} ions.

For $1_{\mathbf{Yb}}$, the increase in the $\Delta_{\mathrm{eff}}/k_B$ value to 44.8 K occurs compared to the K^I–Yb^{III}–V^{IV} compound ($\Delta_{\mathrm{eff}}/k_B = 26$ K), although, in these compounds, the Yb^{III} coordination polyhedra have similar geometry (triangular dodecahedron) and the shortest $Yb\cdots V$ distances are also similar (5.684 Å in K^I–Yb^{III}–V^{IV} and ~5.7 Å in $1_{\mathbf{Yb}}$). Thus, the possible influence of crystal packing and intermolecular interactions on SMM behavior can be assumed in this case.

The literature review showed that 3d-Er^{III} and 3d-Yb^{III} SMMs containing paramagnetic 3d-metal ions are quite rare (Tables 7 and 8). To date, compound $1_{\mathbf{Er}}$ is the first representative of heterometallic V^{IV}–Er^{III} single-molecule magnets. The value of $\Delta_{\mathrm{eff}}/k_B$ calculated for $1_{\mathbf{Er}}$ is comparable with those for compounds with triangular dodecahedral ErO_8 coordination environment (Table 7). Among all reported heterometallic compounds of such type, $1_{\mathbf{Yb}}$ displays the record value of $\Delta_{\mathrm{eff}}/k_B$ (Table 8).

Table 4 The best-fit parameters of magnetization relaxation for $1_{\mathbf{Dy}}$

	Orbach		Orbach + QTM		
	$\Delta_{\mathrm{eff}}/k_B$, K	τ_0, s	$\Delta_{\mathrm{eff}}/k_B$, K	τ_0, s	B, s^{-1}
LF	50.4 ± 0.2	$2.70 \times 10^{-8} \pm 8 \times 10^{-10}$	52 (fixed)	$2.1 \times 10^{-8} \pm 2 \times 10^{-9}$	560 ± 11
HF	26 ± 2	$4 \times 10^{-7} \pm 1 \times 10^{-7}$	39 ± 3	$6 \times 10^{-8} \pm 3 \times 10^{-8}$	9066 ± 294

Table 5 The best-fit parameters of magnetization relaxation for 1_{Er} and 1_{Yb}

Compound	Orbach		Raman + direct			Raman	
	Δ_{eff}/k_B, K	τ_0, s	A_{direct}, K^{-1} Oe^{-4} s^{-1}	C_{Raman}, s^{-1} K^{-n_Raman}	n_Raman	C_{Raman}, c^{-1} K^{-n_Raman}	n_Raman
1_{Er}	19.2 ± 0.2	$1.8 \times 10^{-8} \pm 1 \times 10^{-9}$	—	—	—	41.0 ± 0.5	7 (fixed)
1_{Yb}	44.8 ± 0.5	$5.3 \times 10^{-8} \pm 4 \times 10^{-9}$	$1.20 \times 10^{-11} \pm 2 \times 10^{-13}$	$3.5 \times 10^{-2} \pm 4 \times 10^{-3}$	7 (fixed)	—	—

Table 6 Parameters of slow magnetic relaxation of the reported 3d-Dy^{III} SMMs with paramagnetic 3d-metal ions and triangular dodecahedral DyO_8 coordination environment

Compound	$Dy^{III}O_8$ coordination polyhedron	Δ_{eff}/k_B, K (H_{dc}, Oe)	τ_0, s	Ref.
$[Dy_2^{III}Ni_2^{II}(bpy^{[1]})_2(NO_2\text{-}benz^{[2]})_{10}]$	TDD-8[a]	2.8 (0)	5.47×10^{-6}	23a
$[\{Dy^{III}(hfac^{[3]})_3\}_2\{Ni^{II}(bpca^{[4]})_2\}]\cdot CHCl_3$	TDD-8	4.9 (1000)	1.3×10^{-6}	23b
$[Fe_6^{III}Dy_3^{III}(OMe)_9(vanox^{[5]})_6(Br\text{-}benz^{[6]})_6]$	TDD-8	4.9 (1000)	5.2×10^{-5}	23c
$[Dy_2^{III}Co_6^{II}(OH)_4(L^{[7]})_6(piv^{[8]})_8(MeCN)_2]\cdot0.5CH_2Cl_2$	TDD-8	7.7^d (1000)	5.7×10^{-8}	23d
$[Co_2^{II}(L^{[9]})_2(PhCO_2^{[10]})_2Dy_2^{III}(hfac)_4]$	TDD-8	8.8^d (0)	2.0×10^{-7}	23e
		7.8^d (1000)	3.9×10^{-7}	
$[\{Dy^{III}(hfac)_3\}_2\{Fe^{II}(bpca)_2\}]\cdot CHCl_3$	TDD-8	9.7 (1000)	8.7×10^{-8}	23b
$[Ni_2^{II}Dy_3^{III}(O)(OH)_3(L^{[11]})_3(piv)_3](ClO_4)\cdot8MeCN\cdot3CH_2Cl_2\cdot5.5H_2O$	TDD-8	~10 (3000)	~10^{-6}	23f
$[Ni_2^{II}Dy_2^{III}(CO_3)_2(HL^{[12]})(EtOH)(OAc^{[13]})]\cdot2EtOH$	TDD-8	11.52 (1200)	5.01×10^{-6}	23g
$[Fe_6^{III}Dy_3^{III}(OMe)_9(vanox)_6(benz^{[14]})_6]$	TDD-8	12.4 (2000)	8.0×10^{-5}	23h
$[Co_4^{II}Dy_3^{III}(L^{[15]})_4(piv)_8(OH)(MeOH)_2]\, H_2O\cdot3MeOH$	TDD-8	12.5 (0)	1.51×10^{-6}	23i
$[Dy_2^{III}Ni_2^{II}Mn_2^{III}(L^{[16]})_4(OAc)_2(OH)_4(MeOH)_2](NO_3)_2\cdot2MeOH$	TDD-8	13.0 (0)	2.8×10^{-7}	23j
$[Dy_2^{III}Ni_4^{II}(L^{[16]})_4(OAc)_2(OH)_4(MeOH)_2]\cdot4MeOH$	TDD-8	13.4 (0)	3.4×10^{-7}	23j
$[Dy_4^{III}Ni^{II}(OH)_3(OAc)_4(HL^{[17]})_3](ClO_4)_3\, 3MeOH$	TDD-8 ↔ BTPR-8[b]	7.6 (1200)	7.5×10^{-6}	23k
$[Dy_3^{III}Co_8^{II}(OMe)_2(L^{[18]})_4(HL^{[18]})_2(OAc)_2(NO_3)_2(MeCN)_2]\cdot MeCN\cdot H_2O$	TDD-8	14.89 (0)	1.68×10^{-7}	23l
$[Dy^{III}Fe^{II}(H_2O)(phen^{[19]})(mbenz^{[20]})_5]$	TDD-8	17 (3000)	2.6×10^{-9}	23m
$[Dy^{III}Ni^{II}(H_2O)(phen)(mbenz)_5]$	TDD-8	20 (5000)	1.38×10^{-8}	23m
$[Fe_6^{III}Dy_3^{III}(OMe)_9(vanox)_6(F\text{-}benz^{[21]})_6]$	TDD-8, TDD-8 ↔ SAPR-8[c]	21.3 (1500)	4.1×10^{-7}	23c
$[Dy_2^{III}Ni_2^{II}(bipy)_2(mbenz)_{10}]$	TDD-8	25.9 (0)	1.16×10^{-6}	23a
$[(L^{[22]})Dy^{III}Mn_3^{IV}O_4(OAc)_3(DMF)_2](OTf^{[23]})$	TDD-8	27 (0)	2.13×10^{-8}	23n
$[Cr_2^{III}Dy_2^{III}(OMe)(OH)(4\text{-}^tBubenz^{[24]})_4(^tBudea^{[25]})_2(NO_3)_2]\cdot MeOH\cdot2Et_2O$	TDD-8 ↔ SAPR-8	31.3^e (0)	7.7×10^{-8}	23o
$[Fe_6^{III}Dy_3^{III}(OMe)_9(vanox)_6(Cl\text{-}benz^{[26]})_6]$	TDD-8, TDD-8 ↔ SAPR-8	36.1 (2000)	3.4×10^{-7}	23c
$[Dy_2^{III}Ni_2^{II}(bpy)_2(benz)_{10}]$	TDD-8	39.9 (0)	1.80×10^{-8}	23a
$[NaDy^{III}(V^{IV}O)_2(cbdc)_4(H_2O)_{10}]_n$	**TDD-8**	**LF: 50.4 (1000)**	**2.70×10^{-8}**	**This work**
		HF: 26 (1000)	**4×10^{-7}**	
$[Dy_2^{III}Cu_6^{II}(ipO^{[27]})_6(H_2O)_{12}]_n$	TDD-8	63.68 (2000)	3.77×10^{-8}	23p
$[Mn_4^{IV}Mn_{18}^{III}Dy^{III}O_{20}(OH)_2(piv)_{20}(HCO_2^{[28]})_4(NO_3)_3(H_2O)_7]\cdot5MeNO_2\, H_2O$	TDD-8	74 (0)	2.0×10^{-12}	23q
$[Dy_2^{III}Cr_2^{III}(OH)_2(FcCO_2^{[29]})_4(NO_3)_2(Htea^{[30]})_2]\cdot2MePh^{[31]}\cdot2THF$	TDD-8	75 (0)	26×10^{-9}	23r
$[Ni_6^{II}Dy^{III}(L^{[32]})_8(OAc)_2(NO_3)(OH)_2(OMe)_2]$	TDD-8	122.73 (0)	7.64×10^{-13}	23s

[1] bpy = 2,2′-bipyridine; [2] NO_2-benz⁻ = 3-nitrobenzoate; [3] hfac⁻ = 1,1,1,5,5,5-hexafluoroacetylacetonate; [4] bpca⁻ = bis(2-pyridylcarbonyl)amine; [5] H_2vanox = o-vanillinoxime; [6] Br-benz⁻ = 4-bromobenzoate; [7] HL = 6-chloro-2-pyridinol; [8] piv⁻ = trimethylacetate; [9] H_2L = N,N′-dimethyl-N,N′-bis(2-hydroxy-3,5-dimethylbenzyl)ethylenediamine; [10] $PhCO_2$⁻ = phenylacetate; [11] H_2L = 6,6′-{(2-(dimethylamino)ethylazanediyl)-bis(methylene)}bis(2-hydroxy-4-methylphenol); [12] H_3L = N,N′-bis(3-methoxysalicylidene)-1,3-diamino-2-propanol; [13] OAc⁻ = acetate; [14] benz⁻ = benzoate; [15] H_2L = 2-{[(2-hydroxy-3-methoxybenzylidene)amino]methyl}phenol; [16] H_2L = 2-{[(2-hydroxy-3-methoxybenzyl)imino]methyl}phenol; [17] H_2L = 2-(benzothiazol-2-ylhydrazonomethyl)-6-methoxyphenol; [18] H_3L = ligand formed from the *in situ* condensation reaction of 3-amino-1,2-propanediol with 2-hydroxy-1-naphthaldehyde; [19] phen = 1,10-phenanthroline; [20] mbenz⁻ = 3-methylbenzoate; [21] F-benz⁻ = 4-fluorobenzoate; [22] L = 1,3,5-Tris(2-di(2′-pyridyl)hydroxymethylphenyl)benzene; [23] OTf⁻ = trifluoromethanesulfonate; [24] 4-^{t}Bubenz = 4-*tert*-butylbenzoate; [25] ^{t}BudeaH_2 = N-*tert*-butyldiethanolamine; [26] Cl-benz = 4-chlorobenzoate; [27] ipO⁻ = 2-hydroxyisophthalate; [28] HCO_2⁻ = formate; [29] $FcCO_2$⁻ = ferrocenecarboxylate; [30] teaH_3 = triethanolamine; [31] MePh = toluene; [32] HL = 8-hydroxyquinoline. [a] TDD-8 = triangular dodecahedron. [b] BTPR-8 = bicapped trigonal prism. [c] SAPR-8 = square antiprism. [d] Rough estimation using $\ln(\chi''/\chi') = \ln(2\pi\nu\tau_0) + \Delta_{eff}/k_BT$ equation. [e] Recalculated from cm^{-1}.

EPR spectroscopy of 1_{Yb} and 1_{Dy}

Continuous wave (CW) EPR spectra of 1_{Yb} and 1_{Dy} at room temperature are typical for oxovanadium(IV) complexes and display hyperfine structure of V^{IV} ion (Fig. 6). No signatures of Yb^{III} and Dy^{III} ions are observed at room temperature, but the spectrum is dominated by V^{IV} EPR signal. This signal can be simulated using typical[26] g- and A-tensors (the latter refers to the hyperfine interaction tensors): g = [1.975 1.975 1.938], A =

[185 185 520] MHz for 1_{Dy}, and g = [1.974 1.974 1.941], A = [164 164 521] MHz for 1_{Yb}. Reference compound 1_Y with diamagnetic rare-earth metal ion (Y^{III}) shows almost the same EPR signal of V^{IV} at room temperature and can be simulated using the very similar set of parameters g = [1.974 1.974 1.938], A = [184 184 518] MHz, which agrees well with previous data.[16]

However, as the temperature lowers, EPR spectra of both 1_{Yb} and 1_{Dy} become broader, resulting in one line with unresolved structure at 10 K (Fig. 6). This trend is unusual as most

Table 7 The parameters of slow magnetic relaxation of the reported 3d-Er^{III} SMMs with paramagnetic 3d-metal ions

Compound	Er^{III} environment, coordination polyhedron	Δ_{eff}/k_B, K (H_{dc}, Oe)	τ_0, s	Ref.
$\{[Fe^{III}Er^{III}(CN)_6(2\text{-}PNO^{[1]})_5]\cdot 4H_2O\}_n$	ErN_2O_5, PBPY-7[a]	43.55 (1000)	2.10×10^{-9}	24a
$(Et_3NH)_2[Ni_2^{II}Er_2^{III}(OH)_2(piv^{[2]})_{10}]$	ErO_8, SAPR-8[b]	18 (1000)	3.9×10^{-6}	3
$[Cu_8^{II}Er^{III}(OH)_8(2\text{-}ma^{[3]})_8Cl_2](ClO_4)\cdot 21H_2O$	ErO_8, SAPR-8	22.9 (0)	4.74×10^{-7}	24b
		33 (1000)	9.48×10^{-6}	
$[Fe_2^{III}Er^{III}(OH)(pmide^{[4]})_2(p\text{-}Me\text{-}benz^{[5]})_6]\cdot 2MeCN$	ErN_2O_6, SAPR-8	16.51 (1000)	2.03×10^{-7}	24c
$[Cr^{III}Er_6^{III}(OH)_8(o\text{-}tol^{[6]})_{12}(NO_3)(MeOH)_5]\cdot 2MeOH$	ErO_8, TDD-8[c]	4.5 (3000)	9.1×10^{-8}	24d
$[NaEr^{III}(V^{IV}O)_2(cbdc)_4(H_2O)_{10}]_n$	ErO_8, TDD-8	19.2 (1000)	1.8×10^{-8}	This work
$[Ni_4^{II}Er^{III}(L^{[7]})_2(HL^{[7]})_2(MeCN)_3Cl]\cdot 2H_2O\cdot 2MeCN$	ErO_8, TDD-8	31.87[g] (4000)	7.94×10^{-11}	24e
$[Ni_2^{II}Er^{III}(L^{[8]})(OAc^{[9]})(NO_3)_2(MeCN)]\cdot MeCN$	ErO_9, CSAPR-9[d]	11.91 (1000)	5.12×10^{-8}	24f
$(NMe_4)_2[Cu_3^{II}Er_2^{III}(H_3L^{[10]})_2(NO_3)_7(MeOH)_2](NO_3)$	ErO_9, CSAPR-9	14.8 (0)	1.2×10^{-7}	24g
$[Fe^{II}Er^{III}\{HB(pz)_3\}^{[11]}(CN)_3(NO_3)_2(pyim^{[12]})(Ph_3PO^{[13]})]_2\cdot 2MeCN$	ErN_4O_5, MFF-9[e]	57.6[g] (2500)	—	24h
$[Ni^{II}Er^{III}(L^{[14]})_2(NO_3)_3]\cdot 0.5H_2O$	ErO_{10}, JBCSAPR-10[f]	12.1 (1000)	3.49×10^{-7}	24i

[1]2-PNO = 2-picoline-N-oxide; [2]piv$^-$ = trimethylacetate; [3]2-ma = 2-methylalanine; [4]H_2pmide = N-(2-pyridylmethyl)iminodiethanol; [5]p-Me-benz$^-$ = 4-methylbenzoate; [6]o-tol = o-toluate; [7]H_3L = (E)-2-(hydroxymethyl)-6-(((2-hydroxyphenyl)imino)methyl)-4-methylphenol; [8]H_2L = N,N'-dimethyl-N,N'-bis(2-hydroxy-3-formyl-5-bromo-benzyl)ethylenediamine; [9]OAc$^-$ = acetate; [10]H_6L = 2,2′-(propane-1,3-diyldiimino)bis[2-(hydroxylmethyl)propane-1,3-diol]; [11]{HB(pz)$_3$}$^-$ = hydrotris(pyrazolyl)borate; [12]pyim = 2-(1H-imidazol-2-yl)pyridine; [13]Ph$_3$PO = triphenylphosphineoxide; [14]HL = 3-methoxy-N-[2-(methylsulfanyl)phenyl]salicylaldimine. [a] PBPY-7 = pentagonal bipyramid. [b] SAPR-8 = square antiprism. [c] TDD-8 = triangular dodecahedron. [d] CSAPR-9 = capped square antiprism. [e] MFF-9 = muffin. [f] JBCSAPR-10 = bicapped square antiprism. [g] Recalculated from cm^{-1}.

Table 8 The parameters of slow magnetic relaxation of the reported 3d-Yb^{III} SMMs with paramagnetic 3d-metal ions

Compound	Yb^{III} environment, coordination polyhedron	Δ_{eff}/k_B, K (H_{dc}, Oe)	τ_0, s	Ref.
$\{Yb^{III}(4\text{-}pyridone)_4[Fe^{II}(phen^{[1]})_2(CN)_2]_2\}(OTf^{[2]})_3\cdot 2MeCN$	YbN_2O_4, OC-6[a]	12.5/800	7.28×10^{-6}	25a
$\{Yb^{III}(4\text{-}pyridone)_4[Fe^{II}(phen)_2(CN)_2]_2\}(OTf)_3\cdot 2AcrCN^{[3]}$	YbN_2O_4, OC-6	7.86/800	2.51×10^{-5}	25a
$\{Yb^{III}(4\text{-}pyridone)_4[Fe^{II}(phen)_2(CN)_2]_2\}(OTf)_3\cdot 2PrCN^{[4]}$	YbN_2O_4, OC-6	10.28/800	1.46×10^{-5}	25a
$\{Yb^{III}(4\text{-}pyridone)_4[Fe^{II}(phen)_2(CN)_2]_2\}(OTf)_3\cdot 2MalCN^{[5]}\cdot MeOH$	YbN_2O_4, OC-6	4.83/800	5.82×10^{-5}	25a
$[Na_2Yb_2^{III}Cu_2^{II}(OH)_2(piv^{[6]})_{10}(EtOH)_2]\cdot EtOH$	YbO_8, SAPR-8[b]	8.5/1000	2.1×10^{-6}	14c
$[Yb^{III}\{Cu_4^{II}(butyrat^{[7]})_4\}_2]Cl_3\cdot MeOH\cdot 26H_2O$	YbO_8, SAPR-8	6.84/1000	1.04×10^{-5}	25b
$[Yb^{III}Cu_8^{II}(OH)_8(2\text{-}ma^{[8]})_8(Cl)_2](ClO_4)\cdot 21H_2O$	YbO_8, SAPR-8	22.5/700	1.48×10^{-8}	24b
$\{[KYb(VO)_2(cbdc)_4(H_2O)_{11}]\cdot 2H_2O\}_2$	YbO_8, TDD-8[c]	23/2000	5.6×10^{-7}	6a
$[NaYb(VO)_2(cbdc)_4(H_2O)_{10}]_n$	YbO_8, TDD-8	44.8/2500	5.3×10^{-8}	This work

[1]phen = 1,10-phenanthroline; [2]OTf$^-$ = trifluoromethanesulfonate; [3]AcrCN = acrylonitrile; [4]PrCN = propionitrile; [5]MalCN = malononitrile; [6]piv$^-$ = trimethylacetate; [7]H_2butyrat = 3-aminobutyric hydroxamic acid; [8]2-ma = 2-methylalanine. [a] OC-6 = octahedron. [b] SAPR-8 = square antiprism. [c] TDD-8 = triangular dodecahedron.

relaxation processes become slower at low temperatures, leading to the narrowing of EPR lines. Remarkably, the EPR spectrum of reference compound 1_Y still shows a resolved hyperfine structure at 10 K; therefore, drastic broadening of EPR spectra in cases of 1_{Yb} and 1_{Dy} at 10 K should be assigned to the interactions between V^{IV} and Yb^{III}/Dy^{III} ions. Note that, in addition to V^{IV} signal, the 10 K spectrum of 1_{Yb} shows a small feature at ~100 mT, that is tentatively assigned to the contribution of Yb^{III}.[27]

These interactions are more clearly evident in pulse EPR. In order to complement ac-magnetic susceptibility data and shed light on faster processes on micro- and submicroseconds time-scales, we performed measurements of phase memory time (T_m) for 1_{Yb} and 1_{Dy} at 10–60 K. Two-pulse (Hahn) echo was monitored as a function of interpulse delay, and stretched exponential analysis ($I \propto e^{-\left(\frac{t}{T_m}\right)^\beta}$, $\beta = 2 \pm 0.5$) was then employed to obtain corresponding T_m values.

Fig. 7 shows the obtained $T_m(T)$ dependences for 1_{Yb}, 1_{Dy} and the reference compound of molecular structure $[KY(VO)_2(cbdc)_4(H_2O)_{11}]\cdot 2H_2O$ (M_Y)[6a,16] with diamagnetic rare-earth metal ion (see the ESI† for details and choice of M_Y). The $T_m(T)$ dependence is observed to have a non-monotonous behavior for 1_{Yb} and 1_{Dy}: the relaxation accelerates leading to a decrease of T_m values, reaching minima at $T \sim 10$–12 K. Moreover, reference compound M_Y with diamagnetic Y^{III} ion shows perfectly monotonous dependence without such peculiarity. Again, this means that the observed behavior for 1_{Yb} and 1_{Dy} owes to the interactions between V^{IV} and Yb^{III}/Dy^{III}. This also confirms that the V^{IV}–Yb^{III} and V^{IV}–Dy^{III} units are present when 1_{Yb} and 1_{Dy} are dissolved in water/glycerol, since otherwise their $T_m(T)$ dependences would be similar to that of M_Y.

In fact, such phenomenon is generally known in literature and is called phase relaxation enhancement (PRE), $i.e.$ an increase of the relaxation rate (decrease of T_m) induced by a partner spin coupled with observer spin by dipolar interaction.[28] In compounds 1_{Yb} and 1_{Dy}, we deal with the spins of two types – slow-relaxing $S = 1/2$ spins of V^{IV}, and much faster relaxing spins of Yb^{III} or Dy^{III}. If the spin of lanthanide ion
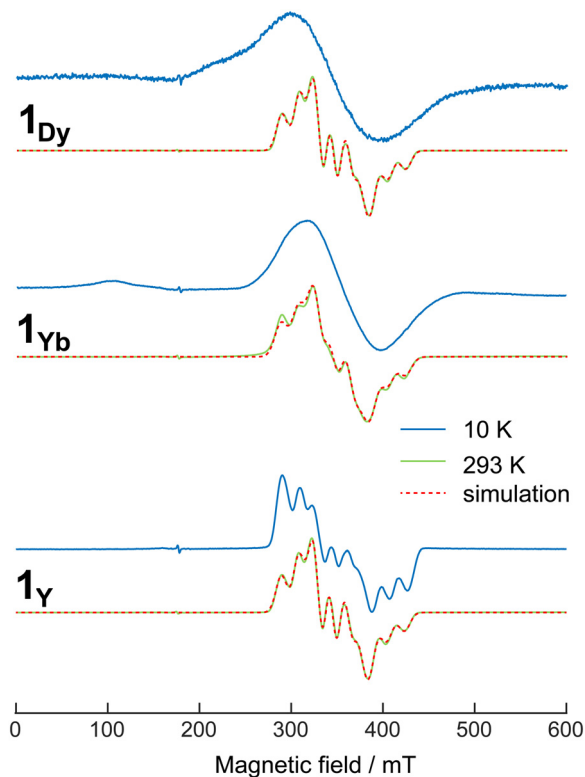
Fig. 6 CW EPR spectra of 1_{Dy}, 1_{Yb} and 1_Y at 293 K and 10 K. Simulations are shown in red.

Fig. 7 $T_m(T)$ dependences for 1_{Yb}, 1_{Dy} and the reference compound M_Y. Solid line guides the eye.

relaxes (flips) much faster than that of vanadium, the dipolar interaction will be averaged and no effect on vanadium EPR should be observed.

This situation corresponds to CW EPR spectra of 1_{Yb} and 1_{Dy} at room temperature and to the $T_m(T)$ dependences at $T > 30$ K. In another limit, if (hypothetically) lanthanide spin relaxed too slowly, there should be no PRE of the vanadium spin as well (this situation is not reached experimentally). However, at intermediate relaxation rate of the lanthanide spins the influence of such fluctuations on the T_m value of vanadium ion is anticipated, due to the dipolar coupling between these ions. At the same time, CW EPR spectrum should broaden due to the contribution of lanthanide.

Previous theoretical consideration of similar phenomena derived general expression for the electron spin echo decay of slow-relaxing spin in the presence of dipolarly-coupled fast-relaxing spin (see ref. 28a):

$$V_{\theta=0}(2\tau) = \left[\left(ch(R\tau) + \frac{W}{R} sh(R\tau) \right)^2 + \frac{A^2(r)}{4R^2} sh^2(R\tau) \right] \exp(-2W\tau),$$

(1)

where $R^2 = W^2 - A^2(r)/4$, $W = \dfrac{1}{2T_1^{Ln}}$ and $A(r_{12}) = \dfrac{g_{1z}g_{2z}\beta^2}{\hbar} \dfrac{(1 - 3\cos^2\theta_{12})}{r_{12}^3}$ with θ_{12} being the angle between $\vec{r}_{12}$ ($\vec{r}_{VLn}$ for the target compounds) and $\vec{B}_0$. In particular, for $R = 0$,
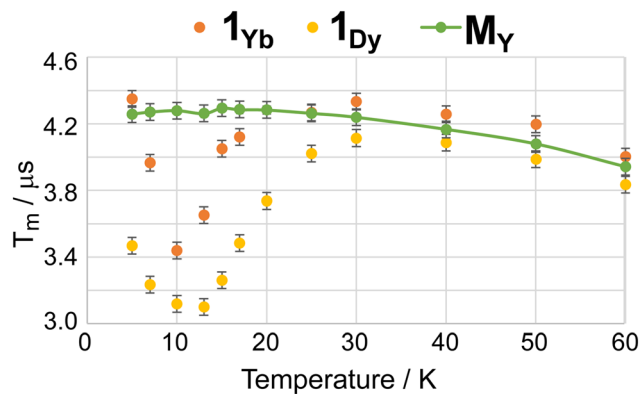
which corresponds to the maximum PRE effect (minimum at $T_m(T)$ dependence), the phase relaxation is enhanced up to:

$$\frac{1}{T_m^{eff}} = \frac{1}{T_m^V} + \frac{1}{T_1^{Ln}}$$

(2)

The eqn (2) qualitatively explains the behavior observed for 1_{Yb} and 1_{Dy} in Fig. 7. The analysis of experimental data allows one to potentially obtain the unique information on spin relaxation times of the lanthanide ions, which are hardly available otherwise being often too short to measure by EPR. However, quantification of this approach requires more work. For instance, eqn (2) should result in a decrease of T_m^{eff} down to $\approx T_1^{Ln}$, which can be estimated as ~10 ns at PRE maximum ($T_1^{Ln} \sim \dfrac{1}{A(r)}$ and $A(r) \sim 200$ MHz in point-dipole approximation based on the crystal structures). This short T_m values are not observed experimentally, meaning that more experimental factors should be theoretically taken into account to describe PRE in Ln^{III}–V^{IV} complexes. First, when 1_{Yb} and 1_{Dy} are dissolved for pulse EPR measurements, one should ensure that there is only one type of spin pairs (or spin triads) present in frozen solution, because if a part of the compound is fully dissolved and separate vanadium, and rare-earth blocks are present, the apparent $T_m(T)$ will have two contributions which should be treated properly. Second, a distribution over parameters T_1^{Ln} and g_z of the pairs (eqn (1)) should be significantly broad[29] and be treated accordingly. The other theoretical challenges are the proper introduction of an atom with strong spin–orbit coupling (relevant for all lanthanides) into the framework of the current PRE-theory and high sensitivity of T_m to the minor changes in the environment.[29] The optimization of the theory might be the topic of our future study. At the same time, the development of clear manifestations of PRE in 1_{Yb} and 1_{Dy} complexes potentially outlooks the use of such phenomena in complex characterization of relaxation times in molecular magnet candidates.

Conclusions

In the Na^I–Ln^{III}–V^{IV} system (Ln^{III} = Tb, Dy, Ho, Er, Tm, Yb) with cyclobutane-1,1-dicarboxylate anions ($cbdc^{2-}$), the lanthanide ionic radius was found to have no impact on the structure of the resulting heterometallic compound. All six new Ln^{III}–V^{IV} compounds obtained have the same 1D polymeric structure formed by trinuclear anionic units $[Ln(VO)_2(cbdc)_4(H_2O)_8]^-$ linked by Na^+ ions.

According to ac-magnetic susceptibility measurements, the Dy^{III}-, Er^{III}-, and Yb^{III}-containing compounds showed field-induced slow relaxation of magnetization. Slow magnetic relaxation observed can be best described by the sum of the Orbach and Raman relaxation mechanisms for Dy^{III}–V^{IV} complex, the sum of Raman and direct relaxation mechanisms for Yb^{III}–V^{IV} complex, and only the Raman relaxation mechanism for Er^{III}–V^{IV} one.

For Dy^{III}–V^{IV}, two relaxation processes were suggested, which may result from the independent relaxation of Dy^{III} and V^{IV} centers and/or possible disorder of water molecules coordinated to Dy^{III}. For complexes with Tb^{III}, Ho^{III}, and Tm^{III} slow magnetic relaxation was not observed due to the possible appearance of weak intramolecular and/or dipole–dipole exchange interactions.

The Er^{III}-containing complex is the first representative of heterometallic Er^{III}–V^{IV} compounds exhibiting slow magnetic relaxation.

For Dy^{III}–V^{IV} and Yb^{III}–V^{IV} studied by EPR spectroscopy, the phenomenon of phase relaxation enhancement (PRE) was observed, which can be used for complex characterization of relaxation times in molecular magnet candidates.

Experimental

Materials and methods

New compounds were synthesized in air, using distilled water as the solvent. Starting reagents included $VOSO_4·3H_2O$ (>99%), $Ba(NO_3)_2$ (>98%), cyclobutane-1,1-dicarboxylic acid (H_2cbdc, 99%, Acros Organics), NaOH (>99%), $Tb(NO_3)_3·6H_2O$ (99.9%, Lanhit), $Dy(NO_3)_3·5H_2O$ (99.9%, Lanhit), $Ho(NO_3)_3·5H_2O$ (99.9%, Lanhit), $Er(NO_3)_3·5H_2O$ (99.9%, Lanhit), $Tm(NO_3)_3·5H_2O$ (99.9%, Lanhit), $Yb(NO_3)_3·5H_2O$ (99.9%, Lanhit).

The infrared spectra of complexes 1_{Ln} were recorded in the frequency range of 4000–400 cm^{-1} on a PerkinElmer Spectrum 65 Fourier transform infrared spectrometer equipped with a Quest ATR Accessory (Specac). Elemental analysis of the compounds synthesized was carried out on a EuroEA 3000 CHNS analyzer (EuroVector, S.p.A.).

The purity of compound samples was approved by powder X-ray diffraction. The patterns were measured on a Bruker D8 Advance diffractometer with a LynxEye detector in the Bragg–Brentano geometry, with the samples dispersed thinly on a zero-background Si sample holder, $\lambda(CuK\alpha)$ = 1.54060 Å, θ/θ scan with variable slits (beam length is 20 mm) in the 2θ-angle range from 5° to 50°, with a step size of 0.020°.

The magnetic properties of compounds 1_{Ln} were studied in the dc- and ac-modes on a Quantum Design PPMS-9 magnetometer in the temperature range of 2–300 K. Dc-magnetic fields with an intensity of 0–5000 Oe and ac-magnetic fields with intensity of 5 Oe, 3 Oe and 1 Oe within frequency ranges 10–100, 100–1000 and 1000–10 000 Hz, respectively, were applied using standard procedure.[30] All magnetic behavior studies were performed using ground polycrystalline samples, sealed in polyethylene bags and frozen in mineral oil to prevent the orientation of crystallites in a magnetic field. The paramagnetic component of the magnetic susceptibility (χ) was determined taking into account the diamagnetic contribution of the sample, evaluated from Pascal's constant, and the diamagnetic contributions of the mineral oil and the sample holder.

All EPR data were collected using Bruker Elexsys E580 spectrometer at X-band (9 GHz) at the Center of Collective Use "Mass spectrometric investigations" SB RAS. The spectrometer was equipped with helium flow cryostat and temperature control system (4–300 K). Continuous wave EPR spectra were obtained on polycrystalline powder samples under conditions avoiding microwave saturation and modulation broadening. Phase memory time was measured using two-pulse Hahn electron spin echo sequence for glassy water/glycerol ($C \sim 0.2$ mM) solutions of target compounds. In all cases samples were placed into quartz sample tubes and studied. Simulations were performed using EasySpin.[31]

General synthesis procedure for $[NaLn(VO)_2(cbdc)_4(H_2O)_{10}]_n$ (1_{Ln}, Ln = Tb, Dy, Ho, Er, Tm, Yb). A weighed sample of $VOSO_4·3H_2O$ (0.100 g, 0.46 mmol) was dissolved in H_2O (15 mL), then $Ba(NO_3)_2$ (0.120 g, 0.46 mmol) was added, and the reaction mixture was stirred for 20 min at 40 °C. The solution of $Na_2(cbdc)$ prepared by neutralization of H_2cbdc (0.133 g, 0.92 mmol) with NaOH (0.074 g, 1.84 mmol) in H_2O (10 mL) was added to the reaction mixture, and the stirring was continued. After 10 min $Ln(NO_3)_3·xH_2O$ (m g, 0.46 mmol) was added. The reaction mixture was stirred for additional 10 min and allowed to stand for 1 hour, then $BaSO_4$ precipitate was removed by filtration. The resulting blue solution (25 mL) was allowed to evaporate slowly in air at 22 °C. X-ray quality blue crystals were obtained within 2 months. The crystals were separated from the mother liquor by filtration, washed with cold H_2O (t = 3 °C) and dried in air at 22 °C.

For 1_{Tb}: x = 6, m = 0.208. The yield was 0.113 g (46.3% based on $VOSO_4·3H_2O$). Anal. Calc for $C_{24}H_{44}NaO_{28}TbV_2$: C, 27.08; H, 4.17. Found: C, 27.01; H, 4.26%. IR (ATR), ν/cm^{-1}: 3642 w, 3348 br. m [$\nu(O–H)$], 3234 m [$\nu(O–H)$], 3000 w [$\nu(C–H)$], 2957 w [$\nu(C–H)$], 1634 m, 1582 s [$\nu_{as}(COO^-)$], 1555 s [$\nu_{as}(COO^-)$], 1443 m, 1431 m, 1391 s [$\nu_s(COO^-)$], 1349 s, 1254 m, 1242 m, 1229 m [$\nu(C–C)_{cycle}$], 1195 w, 1162 w, 1122 m [$\gamma(C(–C)_2)$], 1061 w, 1012 w, 1000 w, 968 s [$\nu(V=O)$], 952 s, 924 s, 875 w, 843 w, 807 w, 773 m, 762 m, 725 s [$\delta(COO^-)$], 647 s, 560 s, 533 s, 471 s, 444 s, 418 s.

For 1_{Dy}: x = 5, y = 0.202. The yield was 0.118 g (47.8% based on $VOSO_4·3H_2O$). Anal. Calc for $C_{24}H_{44}DyNaO_{28}V_2$: C, 26.99; H, 4.15. Found: C, 27.08; H, 4.20%. IR (ATR), ν/cm^{-1}: 3641 vw,

3351 br. m [ν(O–H)], 3229 m [ν(O–H)], 2999 w [ν(C–H)], 2956 w [ν(C–H)], 1631 m, 1581 vs [ν_{as}(COO$^-$)], 1554 vs [ν_{as}(COO$^-$)], 1443 m, 1431 m, 1390 s [ν_s(COO$^-$)], 1348 s, 1254 m, 1242 m, 1229 m [ν(C–C)$_{cycle}$], 1196 w, 1161 w, 1122 m [γ(C(–C)$_2$)], 1061 w, 1012 w, 1000 w, 968 s [ν(V=O)], 952 s, 924 s, 874 w, 843 w, 807 w, 773 m, 762 m, 725 s [δ(COO$^-$)], 649 vs, 604 s, 561 vs, 533 vs, 468 s, 450 vs, 440 vs, 415 s, 403 vs.

For **1$_{Ho}$**: x = 5, y = 0.203. The yield was 0.126 g (51.2% based on VOSO$_4$·3H$_2$O). Anal. Calc for C$_{24}$H$_{44}$HoNaO$_{28}$V$_2$: C, 26.93; H, 4.14. Found: C, 26.90; H, 4.19%. IR (ATR), ν/cm^{-1}: 3641 vw, 3358 br. m [ν(O–H)], 3234 m [ν(O–H)], 3000 w [ν(C–H)], 2957 w [ν(C–H)], 1634 m, 1580 s [ν_{as}(COO$^-$)], 1557 s [ν_{as}(COO$^-$)], 1443 m, 1431 m, 1391 s [ν_s(COO$^-$)], 1349 s, 1254 w, 1242 w, 1230 m [ν(C–C)$_{cycle}$], 1193 w, 1162 w, 1123 m [γ(C(–C)$_2$)], 1061 v.w, 1012 w, 1000 w, 968 s [ν(V=O)], 952 s, 924 m, 875 w, 843 w, 807 w, 773 m, 762 m, 725 s [δ(COO$^-$)], 648 s, 561 s, 533 s, 470 s, 448 s, 438 s, 415 s, 403 vs.

For **1$_{Er}$**: x = 5, y = 0.204. The yield was 0.113 g (45.8% based on VOSO$_4$·3H$_2$O). Anal. Calc for C$_{24}$H$_{44}$ErNaO$_{28}$V$_2$: C, 26.87; H, 4.13. Found: C, 26.79; H, 4.19%. IR (ATR), ν/cm^{-1}: 3641 vw, 3356 br. m [ν(O–H)], 3234 m [ν(O–H)], 3000 w [ν(C–H)], 2957 w [ν(C–H)], 1634 m, 1580 s [ν_{as}(COO$^-$)], 1555 s [ν_{as}(COO$^-$)], 1443 m, 1432 m, 1390 s [ν_s(COO$^-$)], 1348 s, 1254 m, 1242 m, 1229 m [ν(C–C)$_{cycle}$], 1193 w, 1162 w, 1122 m [γ(C(–C)$_2$)], 1063 w, 1012 w, 1000 w, 968 s [ν(V=O)], 953 m, 924 m, 875 w, 843 w, 807 w, 773 m, 762 m, 725 m [δ(COO$^-$)], 650 s, 595 s, 561 s, 532 s, 467 s, 446 s, 437 s, 420 s, 407 vs.

For **1$_{Tm}$**: x = 5, y = 0.205. The yield was 0.077 g (31.2% based on VOSO$_4$·3H$_2$O). Anal. Calc for C$_{24}$H$_{44}$NaO$_{28}$TmV$_2$: C, 26.83; H, 4.13. Found: C, 26.94; H, 4.14%. IR (ATR), ν/cm^{-1}: 3639 vw, 3352 br. m [ν(O–H)], 3238 m [ν(O–H)], 3000 w [ν(C–H)], 2956 w [ν(C–H)], 1634 m, 1583 s [ν_{as}(COO$^-$)], 1557 s [ν_{as}(COO$^-$)], 1443 m, 1431 m, 1391 s [ν_s(COO$^-$)], 1348 s, 1254 m, 1242 m, 1229 m [ν(C–C)$_{cycle}$], 1196 w, 1163 w, 1123 m [γ(C(–C)$_2$)], 1063 w, 1012 w, 1000 w, 968 s [ν(V=O)], 953 s, 924 m, 874 w, 843 w, 807 w, 773 m, 765 m, 725 s [δ(COO$^-$)], 653 s, 595 s, 561 s, 533 s, 471 s, 448 s, 423 s.

For **1$_{Yb}$**: x = 5, y = 0.207. The yield was 0.120 g (48.4% based on VOSO$_4$·3H$_2$O). Anal. Calc for C$_{24}$H$_{44}$NaO$_{28}$V$_2$Yb: C, 26.73; H, 4.11. Found: C, 26.67; H, 4.08%. IR (ATR), ν/cm^{-1}: 3639 vw, 3354 br. m [ν(O–H)], 3229 m [ν(O–H)], 3000 w [ν(C–H)], 2956 w [ν(C–H)], 1634 m, 1582 s [ν_{as}(COO$^-$)], 1554 s [ν_{as}(COO$^-$)], 1443 m, 1431 m, 1391 s [ν_s(COO$^-$)], 1349 s, 1254 m, 1242 m, 1229 m [ν(C–C)$_{cycle}$], 1196 w, 1162 w, 1123 m [γ(C(–C)$_2$)], 1063 w, 1012 w, 1000 w, 968 s [ν(V=O)], 953 s, 924 m, 875 w, 843 w, 807 w, 773 m, 762 m, 726 s [δ(COO$^-$)], 654 s, 561 s, 533 s, 466 s, 448 s, 440 s, 425 s, 416 s.

X-ray crystallography

The X-ray diffraction data sets for compounds **1$_{Dy}$** and **1$_{Er}$** were collected on a Bruker SMART APEX II diffractometer equipped with a CCD detector (Mo-K$_\alpha$, λ = 0.71073 Å, graphite monochromator).[32] A semiempirical absorption correction was applied using SADABS program.[33] The structures were solved by direct methods and refined by the full-matrix least squares with anisotropic displacement parameters for non-hydrogen

Table 9 Crystallographic parameters and structure refinement statistics for compounds **1$_{Dy}$** and **1$_{Er}$**

Parameter	**1$_{Dy}$**	**1$_{Er}$**
Empirical formula	C$_{24}$H$_{44}$DyNaO$_{28}$V$_2$	C$_{24}$H$_{44}$ErNaO$_{28}$V$_2$
Formula weight (g mol^{-1})	1067.96	1072.72
T (K)	150	
Crystal system	Monoclinic	
Space group	$C2/c$	
a (Å)	9.097(2)	9.088(4)
b (Å)	24.739(5)	24.681(11)
c (Å)	17.116(3)	17.098(8)
β (°)	104.682(7)	104.589(8)
V (Å^3)	3726.2(14)	3711(3)
Z	4	4
D_{calc} (g cm^{-3})	1.904	1.920
θ_{min}–θ_{max} (°)	2.97–33.14	2.46–31.83
μ (mm^{-1})	2.59	2.85
No. of measured, independent and observed [$I > 2\sigma(I)$] reflections	7547, 3639, 3336	6910, 3159, 2796
R_{int}	0.026	0.040
GOF	1.045	1.036
R_1^{a}, wR_2^{b} ($I > 2\sigma(I)$)	0.0259, 0.0548	0.0405, 0.0991
R_1^{a}, wR_2^{b} (all data)	0.0298, 0.0567	0.0479, 0.1035
T_{min}, T_{max}	0.626, 0.747	0.456, 0.745
$\Delta\rho_{max}$, $\Delta\rho_{min}$ (e Å^{-3})	0.99, −1.01	1.98, −1.34

^{a} $R_1 = \sum ||F_o| - |F_c||/\sum |F_o|$. ^{b} w$R_2 = [\sum w(F_o^2 - F_c^2)^2/\sum w(F_o^2)^2]^{1/2}$.

atoms. The hydrogen atoms of the OH groups were determined from the difference Fourier maps; with other hydrogen atoms calculated geometrically and refined using a riding model. The calculations were performed with the SHELX-2014 program package[34] *via* OLEX2 1.3 graphical user interface.[35] The crystallographic data for **1$_{Dy}$**, **1$_{Er}$**, and the structure refinement statistics are given in Table 9.

CCDC 2266768 and 2266772† contain the supplementary crystallographic data for **1$_{Dy}$** and **1$_{Er}$**.

Author contributions

Investigation, E. S. B., M. A. S., N. V. G., M. A. K., K. A. B., I. V. K.; formal analysis, E. S. B., M. A. S., N. V. G., M. A. K., K. A. B., I. V. K., M. V. F.; methodology, E. S. B., M. A. S., N. V. G., M. A. K., K. A. B., I. V. K., M. V. F., N. N. E.; visualization, E. S. B., K. A. B., I. V. K., M. V. F.; writing – original draft, E. S. B., M. A. S., K. A. B., N. N. E., M. A. K., I. V. K., M. V. F.; writing – review and editing, E. S. B., N. N. E., M. A. K., M. V. F., I. L. E.; supervision, conceptualization: E. S. B., M. A. K., M. V. F., I. L. E. All authors have read and agreed to the published version of the manuscript.

Data availability

The data supporting this article have been included as part of the ESI.†

Crystallographic data for **1$_{Dy}$** and **1$_{Er}$** have been deposited at the Cambridge Crystallographic Data Centre under CCDC

2266768 and 2266772† numbers and can be obtained from https://www.ccdc.cam.ac.uk/conts/retrieving.html.

Conflicts of interest

There are no conflicts to declare.

Acknowledgements

References

1 A. Dey, J. Acharya and V. Chandrasekhar, Heterometallic 3d–4f Complexes as Single-Molecule Magnets, *Chem. – Asian J.*, 2019, **14**, 4433.

2 S. K. Langley, D. P. Wielechowski, V. Vieru, N. F. Chilton, B. Moubaraki, B. F. Abrahams, L. F. Chibotaru and K. S. Murray, A {$Cr_2^{III}Dy_2^{III}$} Single-Molecule Magnet: Enhancing the Blocking Temperature through 3d Magnetic Exchange, *Angew. Chem., Int. Ed.*, 2013, **52**, 12014.

3 E. Moreno Pineda, N. F. Chilton, F. Tuna, R. E. P. Winpenny and E. J. L. McInnes, Systematic Study of a Family of Butterfly-Like {M_2Ln_2} Molecular Magnets (M = Mg^{II}, Mn^{III}, Co^{II}, Ni^{II}, and Cu^{II}; Ln = Y^{III}, Gd^{III}, Tb^{III}, Dy^{III}, Ho^{III}, and Er^{III}), *Inorg. Chem.*, 2015, **54**, 5930.

4 A. Dey, P. Bag, P. Kalita and V. Chandrasekhar, Heterometallic Cu^{II}–Ln^{III} complexes: Single molecule magnets and magnetic refrigerants, *Coord. Chem. Rev.*, 2021, **432**, 213707.

5 (*a*) N. Subbulakshmi, M. S. Kumar, K. J. Sheela, S. R. Krishnan, V. M. Shanmugam and P. Subramanian, EPR and optical absorption studies of paramagnetic molecular ion (VO^{2+}) in Lithium Sodium Acid Phthalate single crystal, *Physica B*, 2017, **526**, 110; (*b*) Q. H. Le, C. Friebe, W. C. Wang and L. Wondraczek, Spectroscopic properties of Cu^{2+} in alkaline earth metaphosphate, fluoride-phosphate and fluoride-phosphate-sulfate glasses, *J. Non-Cryst. Solids*, 2019, **4**, 100037.

6 (*a*) E. S. Bazhina, G. G. Aleksandrov, M. A. Kiskin, A. A. Korlyukov, N. N. Efimov, A. S. Bogomyakov, A. A. Starikova, V. S. Mironov, E. A. Ugolkova, V. V. Minin, A. A. Sidorov and I. L. Eremenko, The First Series of Heterometallic Ln^{III}-V^{IV} Complexes Based on Substituted Malonic Acid Anions: Synthesis, Structure and Magnetic Properties, *Eur. J. Inorg. Chem.*, 2018, **2018**, 5075; (*b*) K. Kotrle, I. Nemec, J. Moncol, E. Čižmár and R. Herchel, 3d–4f magnetic exchange interactions and anisotropy in a series of heterobimetallic vanadium(IV)–lanthanide(III) Schiff base complexes, *Dalton Trans.*, 2021, **50**, 13883; (*c*) E. S. Bazhina, M. A. Shmelev, K. A. Babeshkin, N. N. Efimov, M. A. Kiskin and I. L. Eremenko, Two families of Ln(III)-V(IV) compounds (Ln (III) = Eu, Tb, Dy, Ho) of different structural types mediated by Rb^+ and Cs^+ cations: Slow magnetic relaxation of Eu(III)- and Ho(III)-containing members, *Polyhedron*, 2023, **236**, 116385.

7 Y.-S. Ding, Y.-F. Deng and Y.-Z. Zheng, The Rise of Single-Ion Magnets as Spin Qubits, *Magnetochemistry*, 2016, **2**, 40.

8 (*a*) S. P. Petrosyants, K. A. Babeshkin, A. V. Gavrikov, A. B. Ilyukhin, E. V. Belova and N. N. Efimov, Towards comparative investigation of Er- and Yb-based SMMs: the effect of the coordination environment configuration on the magnetic relaxation in the series of heteroleptic thiocyanate complexes, *Dalton Trans.*, 2019, **48**, 12644; (*b*) K. A. Babeshkin, A. V. Gavrikov, S. P. Petrosyants, A. B. Ilyukhin, E. V. Belova and N. N. Efimov, Unexpected Supremacy of Non-Dysprosium Single-Ion Magnets within a Series of Isomorphic Lanthanide Cyanocobaltate(III) Complexes, *Eur. J. Inorg. Chem.*, 2020, **2020**, 4380; (*c*) J.-Y. Ge, Z. Chen, H.-Y. Wang, H. Wang, P. Wang, X. Duan and D. Huo, Thiacalix[4]arene-supported mononuclear lanthanide compounds: slow magnetic relaxation in dysprosium and erbium analogues, *New J. Chem.*, 2018, **42**, 17968; (*d*) P. Antal, B. Drahoš, R. Herchel and Z. Trávníček, Muffin-like lanthanide complexes with an N_5O_2-donor macrocyclic ligand showing field-induced single-molecule magnet behaviour, *Dalton Trans.*, 2016, **45**, 15114.

9 S. K. Langley, D. P. Wielechowski, N. F. Chilton, B. Moubaraki and S. Keith, Murray, A Family of {$Cr_2^{III}Ln_2^{III}$} Butterfly Complexes: Effect of the Lanthanide Ion on the Single-Molecule Magnet Properties, *Inorg. Chem.*, 2015, **54**, 10497.

10 (*a*) S.-D. Jiang, S.-S. Liu, L.-N. Zhou, B.-W. Wang, Z.-M. Wang and S. Gao, Series of Lanthanide Organometallic Single-Ion Magnets, *Inorg. Chem.*, 2012, **51**, 3079; (*b*) Y.-S. Meng, Y.-S. Qiao, Y.-Q. Zhang, S.-D. Jiang, Z.-S. Meng, B.-W. Wang, Z.-M. Wang and S. Gao, Can Non-Kramers Tm^{III} Mononuclear Molecules be Single-Molecule Magnets (SMMs)?, *Chem. – Eur. J.*, 2016, **22**, 4704; (*c*) K. L. M. Harriman, I. Korobkov and M. Murugesu, From a Piano Stool to a Sandwich: A Stepwise Route for Improving the Slow Magnetic Relaxation Properties of Thulium, *Organometallics*, 2017, **36**, 4515; (*d*) O. Yu. Mariichak, S. Kaabel, Y. A. Karpichev, G. M. Rozantsev, G. M. Rozantsev, S. V. Radio, C. Pichon, H. Bolvin and J.-P. Sutter, Crystal Structure and Magnetic Properties of Peacock–Weakley Type Polyoxometalates

Na$_9$[Ln(W$_5$O$_{18}$)] (Ln = Tm, Yb): Rare Example of Tm(III) SMM, *Magnetochemistry*, 2020, **6**, 53.

11 D. Banerjee and J. B. Parise, Recent Advances in s-Block Metal Carboxylate Networks, *Cryst. Growth Des.*, 2011, **11**, 4704.

12 (*a*) J. C. Goodwin, D. J. Price, A. K. Powell and S. L. Heath, Alkali Metal Templated Assembly of an Iron Trigonal Prism, *Eur. J. Inorg. Chem.*, 2000, **2000**, 1407; (*b*) W. L. Leong and J. J. Vittal, Alkali metal ion directed self-assembled Ni(II) molecular clusters, *New J. Chem.*, 2010, **34**, 2145; (*c*) S. Gupta, M. V. Kirillova, M. F. C. Guedes da Silva, A. J. L. Pombeiro and A. M. Kirillov, Alkali Metal Directed Assembly of Heterometallic V^V/M (M = Na, K, Cs) Coordination Polymers: Structures, Topological Analysis, and Oxidation Catalytic Properties, *Inorg. Chem.*, 2013, **52**, 8601; (*d*) G. González-Riopedre, M. R. Bermejo, M. I. Fernández-García, A. M. González-Noya, R. Pedrido, M. J. Rodríguez-Doutón and M. Maneiro, Alkali-Metal-Ion-Directed Self-Assembly of Redox-Active Manganese(III) Supramolecular Boxes, *Inorg. Chem.*, 2015, **54**, 2512; (*e*) D. O. Blinou, E. N. Zorina-Tikhonova, J. K. Voronina, M. A. Shmelev, A. K. Matiukhina, P. N. Vasilyev, N. N. Efimov, E. V. Alexandrov, M. A. Kiskin and I. L. Eremenko, Impacts of Alkali Metals on the Structures and Properties of Fe(III) Heterometallic Cyclobutane-1,1-dicarboxylate Complexes, *Cryst. Growth Des.*, 2023, **23**, 5571.

13 Y.-L. Li, H.-L. Wang, Z.-H. Zhu, X.-L. Lu, F.-P. Liang and H.-H. Zou, Alkali metal-linked triangular building blocks assemble a high-nucleation lanthanoid cluster based on single-molecule magnets, *iScience*, 2022, **25**, 105285.

14 (*a*) Y. Maruno, K. Yabe, H. Hagiwara, T. Fujinami, N. Matsumoto, N. Re and J. Mrozinski, yclic and Linear Structures Constructed by Ionic Bonds between Alkali Ion and Pinwheel Pentanuclear [Gd^{III}(Cu^{II}L)$_4$] Core of M[Gd^{III}(Cu^{II}L)$_4$] (M$^+$ = Na$^+$, K$^+$, and Cs$^+$; H$_3$L = N-(4-Methyl-6-oxo-3-azahept-4-enyl)oxamic Acid), *Bull. Chem. Soc. Jpn.*, 2010, **83**, 1511; (*b*) M. R. Azar, T. T. Boron, J. C. Lutter, C. I. Daly, K. A. Zegalia, R. Nimthong, G. M. Ferrence, M. Zeller, J. W. Kampf, V. L. Pecoraro and C. M. Zaleski, Controllable Formation of Heterotrimetallic Coordination Compounds: Systematically Incorporating Lanthanide and Alkali Metal Ions into the Manganese 12-Metallacrown-4 Framework, *Inorg. Chem.*, 2014, **53**, 1729; (*c*) A. A. Bovkunova, E. S. Bazhina, I. S. Evstifeev, Yu. V. Nelyubina, M. A. Shmelev, K. A. Babeshkin, N. N. Efimov, M. A. Kiskin and I. L. Eremenko, Two types of Ln$_2$Cu$_2$ hydroxo-trimethylacetate complexes with 0D and 1D motifs: synthetic features, structural differences, and slow magnetic relaxation, *Dalton Trans.*, 2021, **50**, 12275.

15 E. S. Bazhina, A. A. Korlyukov, J. K. Voronina, K. A. Babeshkin, E. A. Ugolkova, N. N. Efimov, M. V. Fedin, M. A. Kiskin and I. L. Eremenko, Effect of the Alkaline Metal Ion on the Crystal Structure and Magnetic Properties of Heterometallic Gd^{III}-V^{IV} Complexes Based on Cyclobutane-1,1-Dicarboxylate Anions, *Magnetochemistry*, 2021, **7**, 82.

16 I. V. Kurganskii, E. S. Bazhina, A. A. Korlyukov, K. A. Babeshkin, N. N. Efimov, M. A. Kiskin, S. L. Veber, A. A. Sidorov, I. L. Eremenko and M. V. Fedin, Mapping Magnetic Properties and Relaxation in Vanadium(IV) Complexes with Lanthanides by Electron Paramagnetic Resonance, *Molecules*, 2019, **24**, 4582.

17 M. Llunell, D. Casanova, J. Cirera, P. Alemany and S. Alvarez, *SHAPE v.2.1, Program for the Stereochemical Analysis of Molecular Fragments by Means of Continuous Shape Measures and Associated Tools*, Barcelona, Spain, 2013.

18 (*a*) H.-R. Wen, X.-R. Xie, S.-J. Liu, J. Bao, F.-F. Wang, C.-M. Liu and J.-S. Liao, Homochiral luminescent lanthanide dinuclear complexes derived from a chiral carboxylate, *RSC Adv.*, 2015, **5**, 98097; (*b*) M. Gebrezgiabher, Y. Bayeh, T. Gebretsadik, G. Gebreslassie, F. Elemo, M. Thomas and W. Linert, Lanthanide-Based Single-Molecule Magnets Derived from Schiff Base Ligands of Salicylaldehyde Derivatives, *Inorganics*, 2020, **8**, 66.

19 P. Singh, S. Schlittenhardt, D. Thakre, S. K. Kushvaha, S. Kumar, H. S. Karnamkkott, M. Ruben, M. Ibrahim, A. Banerjee and K. C. Mondal, Exploration of Vanadium(IV)-Based Single-Ion Magnet Properties in Diphosphonate-Supported Mixed-Valent Polyoxovanadates, *Cryst. Growth Des.*, 2022, **22**, 5666.

20 (*a*) A. V. Gavrikov, P. S. Koroteev, N. N. Efimov, Z. V. Dobrokhotova, A. B. Ilyukhin, A. K. Kostopoulos, A.-M. Ariciu and V. M. Novotortsev, Novel mononuclear and 1D-polymeric derivatives of lanthanides and (η^6-benzoic acid)tricarbonylchromium: synthesis, structure and magnetism, *Dalton Trans.*, 2017, **46**, 3369; (*b*) A. V. Gavrikov, N. N. Efimov, Z. V. Dobrokhotova, A. B. Ilyukhin, P. N. Vasilyev and V. M. Novotortsev, Novel mononuclear Ln complexes with pyrazine-2-carboxylate and acetylacetonate co-ligands: remarkable single molecule magnet behavior of a Yb derivative, *Dalton Trans.*, 2017, **46**, 11806; (*c*) S. P. Petrosyants, K. A. Babeshkin, A. B. Ilyukhin and N. N. Efimov, Molecular Magnets Based on Mononuclear Aqua and Aqua-Chloro Lanthanide (Tb, Dy, Er, Yb) Complexes with Bipyridine, *Russ. J. Coord. Chem.*, 2021, **47**, 165.

21 (*a*) M. Briganti, F. Santanni, L. Tesi, F. Totti, R. Sessoli and A. Lunghi, *J. Am. Chem. Soc.*, 2021, **143**, 13633; (*b*) L. Gu and R. Wu, Origin of the anomalously low Raman exponents in single molecule magnets, *Phys. Rev. B*, 2021, **103**, 014401.

22 MagSuite v.3.2, M. Rouzières, Zenodo, 2023; DOI: 10.5281/zenodo.4030310 .

23 (*a*) Y. Li, Q. Shang, Y.-Q. Zhang, E.-C. Yang and X.-J. Zhao, Fine Tuning of the Anisotropy Barrier by Ligand Substitution Observed in Linear {Dy$_2$Ni$_2$} Clusters, *Chem. – Eur. J.*, 2016, **22**, 18840; (*b*) F. Pointillart, K. Bernot, R. Sessoli and D. Gatteschi, Effects of 3d–4f Magnetic Exchange Interactions on the Dynamics of the Magnetization of Dy^{III}-M^{II}-Dy^{III} Trinuclear Clusters, *Chem. – Eur. J.*, 2007, **13**, 1602; (*c*) I. A. Kühne, C. E. Anson and

A. K. Powell, The Influence of Halide Substituents on the Structural and Magnetic Properties of Fe_6Dy_3 Rings, *Front. Chem.*, 2020, **8**, 701; (*d*) X.-Q. Zhao, J. Wang, D.-X. Bao, S. Xiang, Y.-J. Liu and Y.-C. Li, The ferromagnetic [Ln_2Co_6] heterometallic complexes, *Dalton Trans.*, 2017, **46**, 2196; (*e*) S. M. T. Abtab, M. C. Majee, M. Maity, J. Titiš, R. Boča and M. Chaudhury, Tetranuclear Hetero-Metal [$Co^{II}_2Ln^{III}_2$] (Ln = Gd, Tb, Dy, Ho, La) Complexes Involving Carboxylato Bridges in a Rare μ_4-η^2:η^2 Mode: Synthesis, Crystal Structures, and Magnetic Properties, *Inorg. Chem.*, 2014, **53**, 1295; (*f*) J. Goura, R. Guillaume, E. Rivière and V. Chandrasekhar, Hexanuclear, Heterometallic, Ni_3Ln_3 Complexes Possessing O-Capped Homo- and Heterometallic Structural Subunits: SMM Behavior of the Dysprosium Analogue, *Inorg. Chem.*, 2014, **53**, 7815; (*g*) L. Jiang, Y. Liu, X. Liu, J. Tian and S. Yan, Three series of heterometallic Ni^{II}–Ln^{III} Schiff base complexes: synthesis, crystal structures and magnetic characterization, *Dalton Trans.*, 2017, **46**, 12558; (*h*) I. A. Kühne, V. Mereacre, C. E. Anson and A. K. Powell, Nine members of a family of nine-membered cyclic coordination clusters; Fe_6Ln_3 wheels (Ln = Gd to Lu and Y), *Chem. Commun.*, 2016, **52**, 1021; (*i*) M. Biswas, E. C. Sañudo and D. Ray, Carboxylate-Decorated Aggregation of Octanuclear Co_4Ln_4 (Ln = Dy, Ho, Yb) Complexes from Ligand-Controlled Hydrolysis: Synthesis, Structures, and Magnetic Properties, *Inorg. Chem.*, 2021, **60**, 11129; (*j*) A. Bhanja, M. Schulze, R. Herchel, E. Moreno-Pineda, W. Wernsdorfer and D. Ray, Selective Coordination of Self-Assembled Hexanuclear [Ni_4Ln_2] and [$Ni_2Mn_2Ln_2$] (Ln = Dy^{III}, Tb^{III}, and Ho^{III}) Complexes: Stepwise Synthesis, Structures, and Magnetic Properties, *Inorg. Chem.*, 2020, **59**, 17929; (*k*) Y. Gao, L. Zhao, X. Xu, G.-F. Xu, Y.-N. Guo, J. Tang and Z. Liu, Heterometallic Cubanes: Syntheses, Structures, and Magnetic Properties of Lanthanide(III)−Nickel(II) Architectures, *Inorg. Chem.*, 2011, **50**, 1304; (*l*) S. Yu, H.-L. Wang, Z. Chen, H.-H. Zou, H. Hu, Z.-H. Zhu, D. Liu, Y. Liang and F.-P. Liang, Two Decanuclear $Dy^{III}_xCo^{II}_{10-x}$ (*x* = 2, 4) Nanoclusters: Structure, Assembly Mechanism, and Magnetic Properties, *Inorg. Chem.*, 2021, **60**, 4904; (*m*) Y. Li, C. Zhang, J.-W. Yu, E.-C. Yang and X.-J. Zhao, Transition metal ion-directed magnetic behaviors observed in an iso-structural heterobinuclear system, *Inorg. Chim. Acta*, 2016, **445**, 110; (*n*) P.-H. Lin, E. Y. Tsui, F. Habib, M. Murugesu and T. Agapie, Effect of the Mn Oxidation State on Single-Molecule-Magnet Properties: Mn^{III} vs Mn^{IV} in Biologically Inspired $DyMn_3O_4$ Cubanes, *Inorg. Chem.*, 2016, **55**, 6095; (*o*) S. K. Langley, D. P. Wielechowski, B. Moubaraki and K. S. Murray, Enhancing the magnetic blocking temperature and magnetic coercivity of {$Cr^{III}_2Ln^{III}_2$} single-molecule magnets *via* bridging ligand modification, *Chem. Commun.*, 2016, **52**, 10976; (*p*) K. Wang, Z.-L. Chen, H.-H. Zou, Z. Zhang, W.-Y. Sun and F.-P. Liang, Two Types of Cu-Ln Heterometallic Coordination Polymers with 2-Hydroxyisophthalate: Syntheses, Structures, and Magnetic Properties, *Cryst. Growth Des.*, 2015, **15**, 2883;

(*q*) C. Papatriantafyllopoulou, W. Wernsdorfer, K. A. Abboud and G. Christou, $Mn_{21}Dy$ Cluster with a Record Magnetization Reversal Barrier for a Mixed 3d/4f Single-Molecule Magnet, *Inorg. Chem.*, 2011, **50**, 421; (*r*) P. S. Koroteev, Z. V. Dobrokhotova, A. B. Ilyukhin, E. V. Belova, A. D. Yapryntsev, M. Rouzières, R. Clérac and N. N. Efimov, Tetranuclear Cr–Ln ferrocenecarboxylate complexes with a defect-dicubane structure: synthesis, magnetism, and thermolysis, *Dalton Trans.*, 2021, **50**, 16990; (*s*) T. Zhang, L.-L. Zhang, C.-X. Ji, S. Ma, Y.-X. Sun, J.-P. Zhao and F.-C. Liu, Construction of Designated Heptanuclear Metal 8-hydroxyquinolates with Different Ions and Auxiliary Coligands, *Cryst. Growth Des.*, 2019, **19**, 3372.

24 (*a*) F. Wang, H.-W. Gong, Y. Zhang, A.-Q. Xue, W.-H. Zhu, Y.-Q. Zhang, Z.-N. Huang, H.-L. Sun, B. Liu, Y.-Y. Fang and S. Gao, The comparative studies on the magnetic relaxation behaviour of the axially-elongated pentagonal-bipyramidal dysprosium and erbium ions in similar one-dimensional chain structures, *Dalton Trans.*, 2021, **50**, 8736; (*b*) G.-J. Zhou, T. Han, Y.-S. Ding, N. F. Chilton and Y.-Z. Zheng, Metallacrowns as Templates for Diabolo-like {$LnCu_8$} Complexes with Nearly Perfect Square Antiprismatic Geometry, *Chem. – Eur. J.*, 2017, **23**, 15617; (*c*) Y. Peng, V. Mereacre, C. E. Anson and A. K. Powell, Butterfly $M^{III}_2Er_2$ (M^{III} = Fe and Al) SMMs: Synthesis, Characterization, and Magnetic Properties, *ACS Omega*, 2018, **3**, 6360; (*d*) K. R. Vignesh, S. K. Langley, A. Swain, B. Moubaraki, M. Damjanović, W. Wernsdorfer, G. Rajaraman and K. S. Murray, Slow Magnetic Relaxation and Single-Molecule Toroidal Behaviour in a Family of Heptanuclear {$Cr^{III}Ln^{III}_6$} (Ln=Tb, Ho, Er) Complexes, *Angew. Chem., Int. Ed.*, 2018, **57**, 779; (*e*) P. Shukla, S. Roy, D. Dolui, W. Cañón-Mancisidor and S. Das, Syntheses, Structures, and Magnetic Properties of Pentanuclear Spirocyclic Ni_4Ln Derivative: Field Induced Slow Magnetic Relaxation by Dysprosium and Erbium Analogue, *Eur. J. Inorg. Chem.*, 2020, **2020**, 823; (*f*) I. Oyarzabal, E. Echenique-Errandonea, E. San Sebastián, A. Rodríguez-Diéguez, J. M. Seco and E. Colacio, Synthesis, Structural Features and Physical Properties of a Family of Triply Bridged Dinuclear 3d-4f Complexes, *Magnetochemistry*, 2021, **7**, 22; (*g*) M. J. Heras Ojea, V. A. Milway, G. Velmurugan, L. H. Thomas, S. J. Coles, C. Wilson, W. Wernsdorfer, G. Rajaraman and M. Murrie, Enhancement of Tb^{III}–Cu^{II} Single-Molecule Magnet Performance through Structural Modification, *Chem. – Eur. J.*, 2016, **22**, 12839; (*h*) M.-G. Alexandru, D. Visinescu, B. Cula, S. Shova, R. Rabelo, N. Moliner, F. Lloret, J. Cano and M. Julve, A rare isostructural series of 3d–4f cyanido-bridged heterometallic squares obtained by assembling [Fe^{III}{$HB(pz)_3$}$(CN)_3$]⁻ and Ln^{III} ions: synthesis, X-ray structure and cryomagnetic study, *Dalton Trans.*, 2021, **50**, 14640; (*i*) B. Dutta, T. Guizouarn, F. Pointillart, K. Kotrle, R. Herchel and D. Ray, Lanthanoid coordination prompts unusually distorted pseudo-octahedral Ni^{II} coordination in heterodinuclear Ni–Ln complexes: synthesis, structure and

understanding of magnetic behaviour through experiment and computation, *Dalton Trans.*, 2023, **52**, 10402.

25 (*a*) M. Liberka, K. Boidachenko, J. J. Zakrzewski, M. Zychowicz, J. Wang, S. Ohkoshi and S. Chorazy, Near-Infrared Emissive Cyanido-Bridged {YbFe$_2$} Molecular Nanomagnets Sensitive to the Nitrile Solvents of Crystallization, *Magnetochemisty*, 2021, **7**, 79; (*b*) W.-W. Chang, H. Yang, H.-Q. Tian, D.-C. Li and J.-M. Dou, 3d–4f Metallacrown complexes with a new sandwich core: synthesis, structures and single molecule magnet behavior, *New J. Chem.*, 2020, **44**, 14145.

26 (*a*) M. Atzori, E. Morra, L. Tesi, A. Albino, M. Chiesa, L. Sorace and R. Sessoli, Quantum Coherence Times Enhancement in Vanadium(IV)-based Potential Molecular Qubits: the Key Role of the Vanadyl Moiety, *J. Am. Chem. Soc.*, 2016, **138**, 11234; (*b*) V. Lagostina, E. Romeo, A. M. Ferrari, V. Maurino and M. Chiesa, Monomeric (VO^{3+}) and dimeric mixed valence (V$_2$O$_3^{3+}$) vanadium species at the surface of shape controlled TiO$_2$ anatase nano crystals, *J. Catal.*, 2022, **406**, 28.

27 C. Bonardi, C. J. Magon, E. A. Vidoto, M. C. Terrile, L. E. Bausá, E. Montoya, D. Bravo, A. Martín and F. J. López, EPR spectroscopy of Yb^{3+} in LiNbO$_3$ and Mg: LiNbO$_3$, *J. Alloys Compd.*, 2001, **323–324**, 340.

28 (*a*) K. M. Salikhov, S. A. Dzuba and A. M. Raitsimring, The theory of electron spin-echo signal decay resulting from dipole-dipole interactions between paramagnetic centers in solids, *J. Magn. Reson.*, 1981, **42**, 255; (*b*) W. Hilczer, J. Goslar, M. Gramza, S. K. Hoffmann, W. Blicharski, A. Osyczka, B. Turyna and W. Froncisz, A resonance enhancement of the phase relaxation in the electron spin echo of nitroxide covalently attached to cytochrome c, *Chem. Phys. Lett.*, 1995, **247**, 601; (*c*) P. R. Vennam, N. Fisher, M. D. Krzyaniak, D. M. Kramer and M. K. Bowman, A Caged, Destabilized, Free Radical Intermediate in the Q-Cycle, *ChemBioChem*, 2013, **14**, 1745.

29 P. Lueders, S. Razzaghi, H. Jäger, R. Tschaggelar, M. A. Hemminga, M. Yulikov and G. Jeschke, Distance determination from dysprosium induced relaxation enhancement: a case study on membrane-inserted WALP23 polypeptides, *Mol. Phys.*, 2013, **111**, 2824–2833.

30 N. N. Efimov, K. A. Babeshkin and A. V. Rotov, Method of dynamic magnetic susceptibility in the study of coordination compounds, *Russ. J. Coord. Chem.*, 2024, **50**, 363.

31 S. Stoll and A. Schweiger, EasySpin, a comprehensive software package for spectral simulation and analysis in EPR, *J. Magn. Reson.*, 2006, **178**, 42.

32 *SMART (control) and SAINT (integration) Software. Version 5.0*, Bruker AXS, Inc., Madison (WI, USA), 1997.

33 G. M. Sheldrick, *SADABS, Program for Scaling and Correction of Area Detector Data*, Göttingen University, Göttingen, Germany, 1997.

34 G. M. Sheldrick, Crystal structure refinement with SHELXL, *Acta Crystallogr., Sect. A: Found. Crystallogr.*, 2015, **71**, 3.

35 O. V. Dolomanov, L. J. Bourhis, R. J. Gildea, J. A. K. Howard and H. Puschmann, OLEX2: a complete structure solution, refinement and analysis program, *J. Appl. Crystallogr.*, 2009, **42**, 339.